A microstructural imprint of melt impregnation in slow spreading lithosphere: Olivine-rich troctolites from the Atlantis Massif, Mid-Atlantic Ridge, 30 degrees N, IODP Hole U1309D

Marion Drouin, Benoit Ildefonse, Marguerite Godard

Geochemistry Geophysics Geosystems G3

Article
Volume 11, Number 6
4 June 2010
Q06003, doi:10.1029/2009GC002995
ISSN: 1525-2027

Published by AGU and the Geochemical Society

A microstructural imprint of melt impregnation in slow spreading lithosphere: Olivine-rich troctolites from the Atlantis Massif, Mid-Atlantic Ridge, 30°N, IODP Hole U1309D

Marion Drouin
Géosciences Montpellier, Université Montpellier 2, CNRS, CC 60, F-34095 Montpellier CEDEX 5, France

Now at Laboratoire Géosciences Réunion, UMR 7154, Université de la Réunion, Institut de Physique du Globe de Paris, CNRS, 15 avenue René Cassin, BP 7151, F-97715 Saint-Denis Messag CEDEX 9, France (marion.drouin@univ-reunion.fr)

Benoit Ildefonse and Marguerite Godard
Géosciences Montpellier, Université Montpellier 2, CNRS, CC 60, F-34095 Montpellier CEDEX 5, France

[1] The 1415 m deep IODP Hole U1309D (Mid-Atlantic Ridge, 30°N) is the second deepest hole drilled into slow spreading oceanic lithosphere. The recovered section comprises essentially gabbroic rocks, with a large range of compositions. The most primitive end-members of the gabbroic sequence, herein referred to as olivine-rich troctolites (ol > ~70%), have textures and geochemical compositions intermediate between that of mantle peridotites and primitive cumulates, indicative of melt impregnation processes. We carried out a detailed microstructural study to further characterize the petrogenetic processes leading to their formation, as well as discuss their mode of emplacement and relationship with neighboring mantle lithosphere. In olivine-rich troctolites, olivines range from coarse-grained subhedral crystals, commonly containing well-developed subgrains, to medium-grained rounded crystals with fewer or no substructures. They are embedded in large, undeformed pyroxene and plagioclase poikiloblasts. Olivine substructures reveal dislocation creep that is consistent with activation of the main high-temperature slip systems, dominantly (010)[100]. Olivine crystallographic preferred orientation is very weak but generally shows a relatively stronger, uncommon [001] concentration. These unusual olivine fabrics are interpreted as resulting from melt impregnation of a previously deformed olivine matrix: the solid olivine framework is disrupted by olivine corrosion along grain and subgrain boundaries, and the high-temperature plastic fabric is modified in a liquid-dominated regime. Based on mineral composition and fabrics and in comparison with what is observed in impregnated mantle rocks elsewhere, we posit that olivine represents relicts of mantle peridotites disaggregated by large melt influx, although the mantle origin of olivine is not unequivocally demonstrated yet. Whatever the initial lithology, impregnation by large volumes of melt has strongly modified the original composition and microstructure. If the mantle origin hypothesis is correct, the original olivine fabric could have been efficiently weakened by dunitization prior to disruption of the olivine framework by melt impregnation. Incorporation, at the base of the lithosphere, of small slivers of impregnated dunite into gabbroic sections, trapped between successive igneous units, may be a common mechanism of lower crustal accretion at slow spreading ridges. Extensive melt-rock interaction processes are expected to contribute significantly to the final chemical composition of erupted lavas.

Components: 10,900 words, 8 figures, 1 table.

Keywords: Integrated Ocean Drilling Program; Atlantis Massif; troctolite; crystallographic preferred orientations; melt impregnation; oceanic lithosphere.

Index Terms: 3035 Marine Geology and Geophysics: Midocean ridge processes; 3036 Marine Geology and Geophysics: Ocean drilling; 8030 Structural Geology: Microstructures.

Received 7 December 2009; **Revised** 1 April 2010; **Accepted** 20 April 2010; **Published** 4 June 2010.

Drouin, M., B. Ildefonse, and M. Godard (2010), A microstructural imprint of melt impregnation in slow spreading lithosphere: Olivine-rich troctolites from the Atlantis Massif, Mid-Atlantic Ridge, 30°N, IODP Hole U1309D, *Geochem. Geophys. Geosyst.*, *11*, Q06003, doi:10.1029/2009GC002995.

1. Introduction

[2] Melt impregnation is commonly observed in mantle rocks at slow [e.g., *Girardeau and Franchetau*, 1993; *Cannat et al.*, 1997; *Seyler and Bonatti*, 1997; *Kelemen et al.*, 2004], and fast spreading ridges [e.g., *Cannat et al.*, 1990; *Hékinian et al.*, 1993; *Allan and Dick*, 1996; *Arai and Matsukage*, 1996; *Dick and Natland*, 1996], as well as in ophiolites [e.g., *Nicolas and Prinzhofer*, 1983; *Boudier*, 1991; *Rampone et al.*, 1997, 2008; *Piccardo et al.*, 2007]. Melt impregnation is associated with pervasive melt/rock interaction involving high melt volumes, and results in the crystallization of significant amount of plagioclase and/or clinopyroxene in peridotite. It occurs in the shallowest part of the mantle, mostly at the mantle/crust transition [e.g., *Boudier and Nicolas*, 1995; *Dijkstra et al.*, 2003; *Borghini et al.*, 2007]. Recent studies indicate that similar magmatic processes may affect crystallizing gabbroic sections at slow spreading ridges [*Lissenberg and Dick*, 2008]. Melt impregnation strongly modifies the composition of impregnated mantle rocks [e.g., *Takazawa et al.*, 2007], which then have compositions intermediate between those of abyssal peridotites and primitive gabbros [e.g., *Niu and Hekinian*, 1997; *Paulick et al.*, 2006; *Godard et al.*, 2009]. Pervasive melt/rock interaction also leads to significant changes in the physical properties and microstructures of mantle rocks, as documented at the asthenosphere/lithosphere transition above mantle plumes [*Tommasi et al.*, 2004] and in peridotite massifs [e.g., *Lenoir et al.*, 2001; *Vauchez and Garrido*, 2001].

[3] Olivine-rich troctolites drilled during Expeditions IODP 304–305 in the Atlantis Massif (Mid-Atlantic Ridge, 30°N) were sampled within a 1415 m thick gabbroic section. The bulk geochemistry of these rocks is intermediate between that of peridotite and that of gabbro [*Godard et al.*, 2009]. *Drouin et al.* [2009] conclude from mineral chemical composition analysis that olivine-rich troctolites have formed in a domain of large magmatic transfer and accumulation, similar to what is described in the mantle-crust transition zone in ophiolites and at fast spreading ridges. In order to investigate the effect of melt/rock reaction and crystallization on mineral Crystallographic Preferred Orientations (CPO), and discuss further the origin of olivine-rich troctolites, we performed microstructural analysis of olivine-rich troctolites, and of neighboring troctolites and olivine gabbros collected from 3 olivine-rich troctolite intervals along IODP Hole U1309D.

2. Atlantis Massif and IODP Hole 1256D

[4] The Atlantis Massif is a ~2 Ma old Oceanic Core Complex (OCC) that is located at 30°N at the inside corner of the eastern intersection of the Mid-Atlantic Ridge with the Atlantis Transform Fault (Figure 1a). It is the result of low-angle detachment faulting [e.g., *Cann et al.*, 1997; *Blackman et al.*, 2002; *Karson et al.*, 2006; *Ildefonse et al.*, 2007], and extends approximately 20 km parallel to the ridge and 15 km across (Figure 1a). The oceanic crust in this type of area along slow spreading ridges is presumably highly heterogeneous with discrete gabbroic bodies intruded into variously serpentinized peridotites [e.g., *Cannat*, 1993, 1996; *Ildefonse et al.*, 2007].

[5] IODP Hole U1309D, the main hole drilled during IODP Expeditions 304–305, is located at the top of the central dome of Atlantis Massif (Figure 1a) where the seafloor coincides with a corrugated detachment fault surface [*Blackman et al.*, 2006]. Hole U1309D penetrated 1415.5 m below seafloor (mbsf) in basement and recovered mostly gabbroic rocks (Figure 1b). The whole core

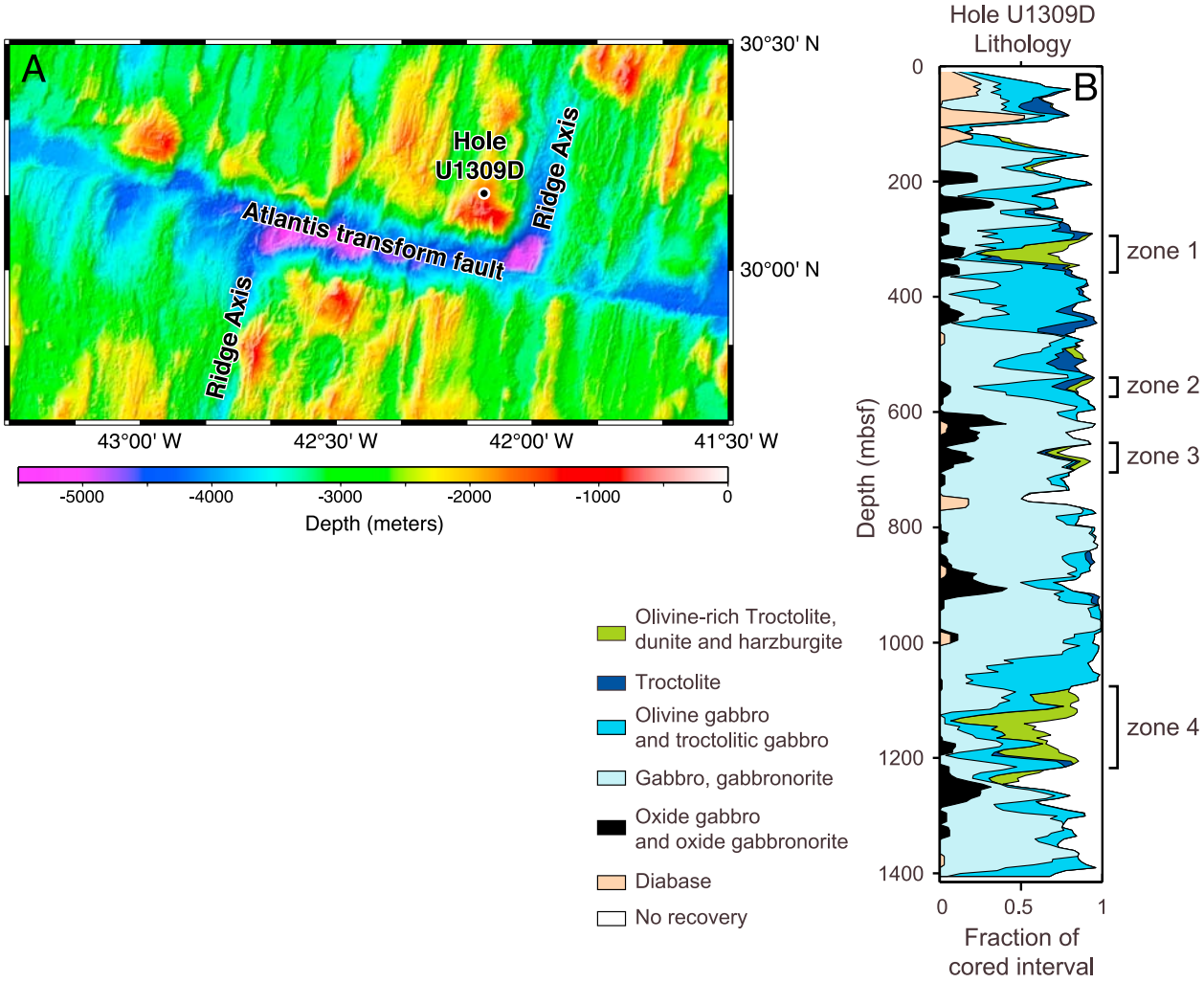

Figure 1. (a) Bathymetric map of the Atlantis Massif area, with the location of IODP Hole U1309D drilled during expedition IODP 304–305 [*Blackman et al.*, 2008]. (b) Lithologies recovered in Hole U1309D, 20 m running average [*Blackman et al.*, 2006], and depth localization of the sampled olivine-rich intervals. Zones 1 to 4 are those sampled by *Drouin et al.* [2009]. The samples studied herein are from zones 1, 2, and 4 (Table 1).

in Hole U1309D is moderately altered at conditions ranging from granulite to zeolite facies. Overall, the alteration tends to decrease downhole. Magmatic deformation associated with the emplacement of Hole U1309D gabbroic intrusive suite is weak and affects only 22% of the recovered core. High-temperature (amphibolite to granulite facies) deformation is rare and high-strain ductile shear zones represent less than 3% of the recovered core.

[6] Minor peridotite (≪1% of the recovered rocks), occurring as intervals a few tens of cm thick was sampled in the upper ~200 m at Site U1309 (Figure 1b). They are described as impregnated peridotites, and interpreted as relicts of mantle lithosphere, intruded and crosscut by gabbroic intrusions [*Tamura et al.*, 2008; *Godard et al.*, 2009]. Diabase intrusions (2.9% of the recovered rocks) of variable thickness (a few cm to several m) occur throughout the entire core; they are more abundant in the upper 130 m (Figure 1b), and have MORB compositions [*Godard et al.*, 2009].

[7] Gabbro is the most abundant recovered rock (56%) with important variations in grain size and modal composition on a decimeter scale. Orthopyroxene was identified in thin sections in many (>5%) gabbro intervals, mostly below 600 mbsf. Olivine gabbro (Ol > 5%) locally grades to troctolitic gabbro and troctolite, and represents the second most abundant recovered rock type (28%). Oxide gabbro (>2% modal Fe-Ti oxides) represents 7% of the recovered rocks and occurs as disseminated patches, as dikelets crosscutting other lithologies,

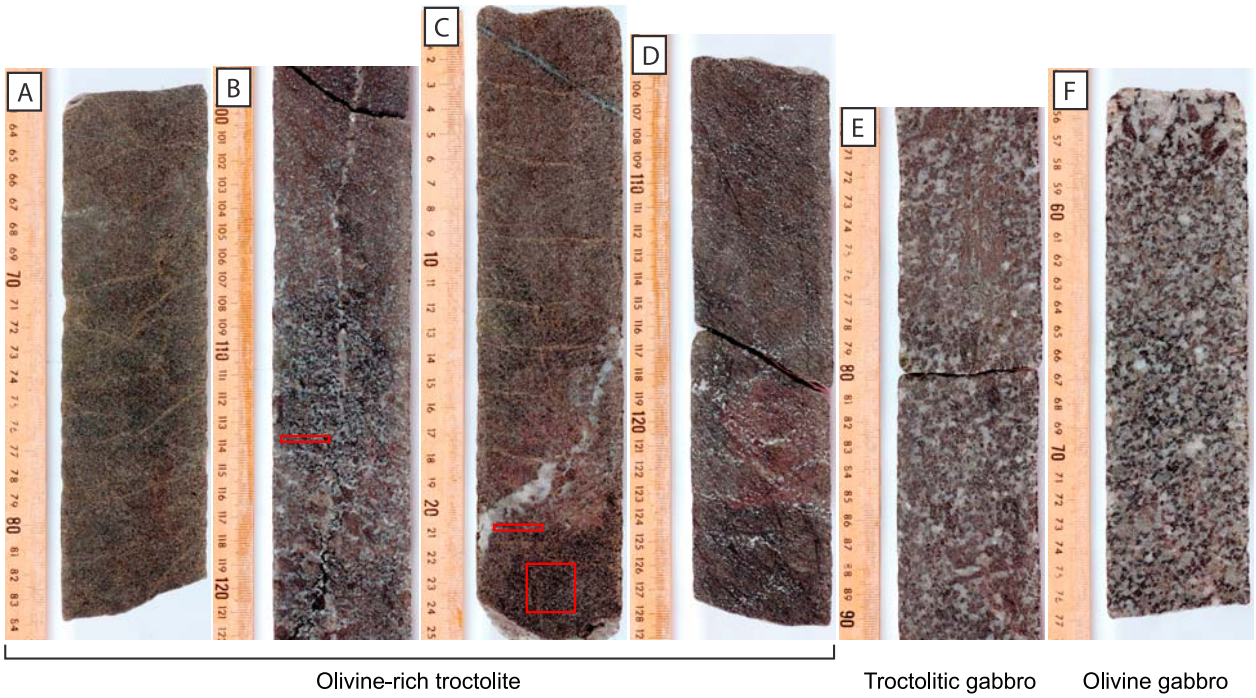

Figure 2. Examples of recovered cores of (a–d) olivine-rich troctolite, (e) troctolitic gabbro, and (f) olivine gabbro. Figure 2a shows core 227R3, 63 to 83 cm. Figure 2b shows core 232R1, 99 to 122 cm. Note the small-scale gradation in plagioclase content. Figure 2c shows core 248R2, 0 to 25 cm, crosscut by a centimeter thick gabbroic vein. Figure 2d shows core 256R2, 105 to 128 cm. Note the heterogeneous distribution of interstitial plagioclase, forming a pervasive, anastomosing network. Figure 2e shows core 251R1, 70 to 91 cm. Figure 2f shows core 268R2, 55 to 77 cm. Red areas indicate the localizations of three samples (Table 1): thin rectangles indicate thin sections perpendicular to the core axis, and square is parallel to the core axis.

or less commonly, associated with ductile deformation zones [*Blackman et al.*, 2006].

[8] Olivine-rich troctolites (Figure 2) represent an olivine-rich (ol > 70%) subset of gabbroic samples. Their modal composition varies at the scale of a few centimeters to a few decimeters; they comprise troctolite, as well as dunite and wehrlite at a very local scale. Olivine-rich troctolites (see rationale for using the term "olivine-rich troctolite" by *Blackman et al.* [2006]) represent 5.4% of the recovered rocks in Hole U1309D (Figure 1b). Olivine-rich troctolites display a distinctive, homogeneous cumulate-like texture with rounded olivine embedded in poikiloblastic clinopyroxene and/or plagioclase (Figures 3a–3f), which resembles those commonly described in layered cumulate series (e.g., the Rum Intrusion [*Holness et al.*, 2007]). The mineral chemistry of olivine-rich troctolites was analyzed in detail by *Drouin et al.* [2009]. Clinopyroxene is high Mg # augite (Mg # 87) and plagioclase anorthite content is 77. Clinopyroxene and plagioclase cores are depleted in trace elements (e.g., Yb_{cpx} ~5–11 × C1-Chondrite [*Sun and McDonough*, 1989]) and they are in equilibrium with MORB-type melts. Olivine has high forsterite contents ranging from 82 to 88, and is in Mg–Fe equilibrium with clinopyroxene. However, its strongly fractionated trace element composition (e.g., Gd/Yb = 0.01–0.02 × C1-Chondrite) is not in equilibrium with neighboring clinopyroxene and plagioclase.

[9] Olivine-rich troctolites are observed in 22 discrete intervals in Hole U1309D, ranging from ~40 cm to ~12 m in thickness, with an average recovery of 75%. These olivine-rich rocks are commonly intruded by thin (~1 to 20 cm) gabbroic intrusions, and are intercalated with olivine and troctolitic gabbro intervals in a given olivine-rich zone (Figures 1b and 2), of which three have been sampled for this study (Table 1). Olivine-rich troctolite is the dominant lithology between 1090 and 1236 mbsf and is locally very fresh (down to <1% serpentinization).

[10] We sampled olivine-rich troctolites, and associated troctolites and olivine gabbros, in three of the four olivine-rich zones defined and analyzed by *Drouin et al.* [2009]. We collected 4 samples in a first interval from ~301 to 363 mbsf (1 olivine-rich troctolite, 2 troctolites and 1 olivine gabbro),

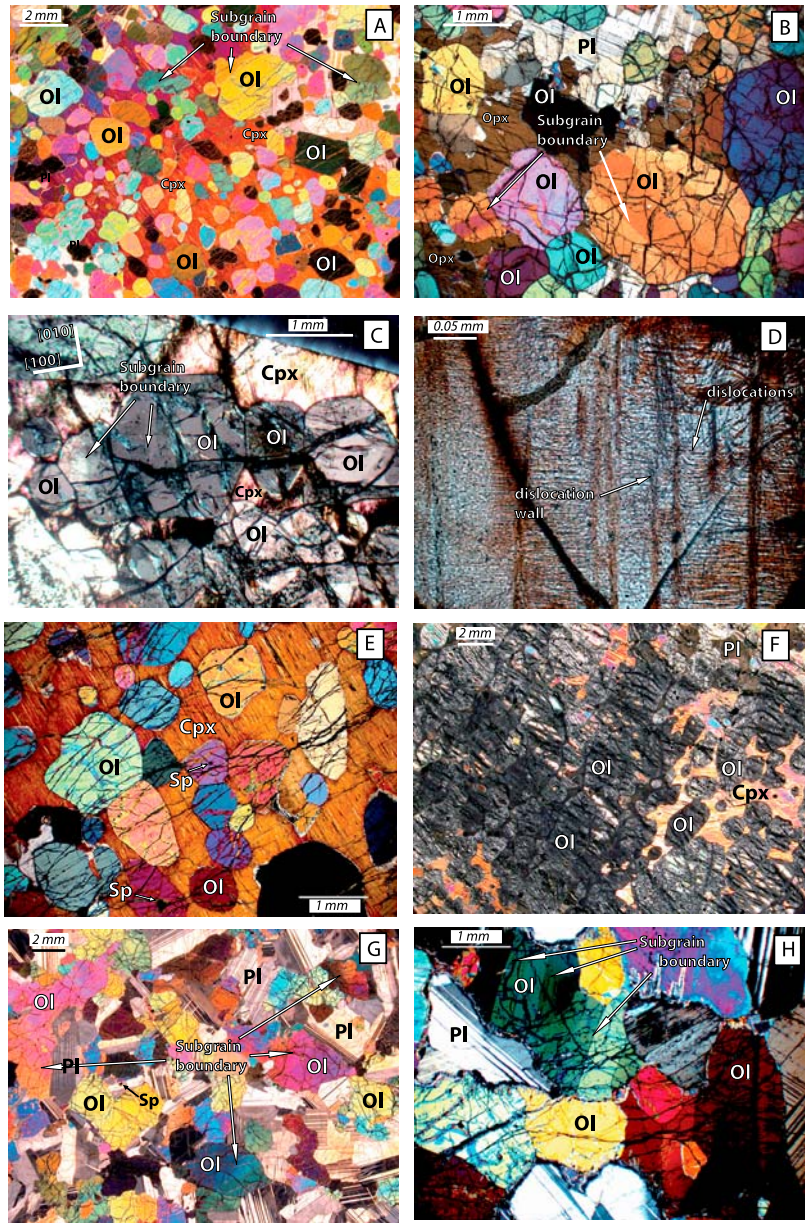

Figure 3. Photomicrographs of representative microstructures in olivine-rich troctolites, troctolites, and olivine gabbros. (a) Rounded and subhedral olivine crystals (Ol) included in large clinopyroxene (Cpx) and plagioclase poikiloblasts forming poikilitic texture in olivine-rich troctolite (sample 247R3_16–18). (b) Coarse-grained subhedral olivine crystals with smooth edges and well-defined and widely spaced subgrain boundaries and poikiloblastic plagioclase (Pl) and orthopyroxene (Opx) (sample 248R2_22–24). (c) Olivines crystals in optical subcontinuity showing curviplanar boundaries and (100) subgrain boundaries in olivine-rich troctolite (sample 247R3_62–66). (d) Detail of dislocation substructures in deformed olivine of olivine-rich troctolite (decorated sample 248R2_18–21). (e) Chains of corroded olivines and rounded olivines embedded in a clinopyroxene oikocryst in olivine-rich troctolite. Spinel (Sp) occurs as small subhedral crystals with polygonal shape, included in olivine (sample 247R3_16–18). (f) Interstitial grains of clinopyroxene and plagioclase forming pervasive textures in olivine-rich troctolite (sample 64R1_58–60). Olivine crystals in this sample are highly serpentinized (g) Olivine crystals showing (100) subgrains boundaries and subhedral laths of plagioclase in a troctolite. Spinel occurs as small subhedral grain between olivine and plagioclase crystals (sample 251R1_87–89). (h) Well-defined subgrain boundaries in olivine from olivine gabbro (sample 117R1_55–57). Figures 3a, 3b, and 3e–3h show cross-polarized light; Figures 3c and 3d show plane-polarized light.

Table 1. General Characteristics of Studied Samples From IODP Hole U1309D[a]

Sample	Ol-Rich Zone	Depth (mbsf)	Rock Type	J Index		Misorientation (<15°) Preferred Rotation Axis	Modal Composition			
				Gridded Data (One Measurement per Grid Node)	Detected Grains (One Measurement per Grain)		Ol (%)	Pl (%)	Cpx (%)	Sp (%)
60R3_39–42	1	313.22	Ol-rich troctolite	10.87	-	[010]	70.5	13	16	0.5
70R2_99–103	1	359.68	troctolite	6.83	-	[010] and [001]	58	39.5	2	0.5
89R1_92–94	1	444.72	Ol-gabbro	7.52	7.13	[001]	27	38	35	0
90R3_8–10	1	451.68	Troctolite	5.46	3.74	[010] and [001]	56	41.5	2	0.5
112R1_69–73	2	554.89	Ol-rich troctolite	6.46	-	[001]	77.5	20	2	0.5
117R1_55–57	2	578.75	Ol-gabbro	7.65	4.15	[001]	26	40	34	0
227R3_121–124	4	1096.14	Ol-rich troctolite	2.18	1.83	undetermined	72.5	13	14	0.5
227R3_124–126	4	1096.17	Ol-rich troctolite	1.67	1.61	undetermined	85	12	2.5	0.5
232R1_112–116	4	1116.22	troctolite	3.57	2.35	[010] and [001]	59	36.5	4	0.5
233R3_21–24	4	1123.06	Ol-rich troctolite	1.63	1.75	undetermined	82	15	2.5	0.5
234R1_22–26	4	1124.92	Ol-rich troctolite	2.37	1.77	[010] and [001]	82	15	2.5	0.5
234R1_27–29	4	1124.97	Ol-rich troctolite	4.33	2.91	[001]	80	15	4.5	0.5
234R3_14–18	4	1127.74	Ol-rich troctolite	2.77	1.98	[010]	83	11.5	5	0.5
235R2_85–89	4	1131.61	Ol-rich troctolite	2.21	2.19	undetermined	82.5	11	6	0.5
237R2_40–43	4	1140.92	Ol-rich troctolite	2.69	3.02	[001]	81	14.5	4	0.5
241R2_94–97	4	1160.71	Ol-rich troctolite	2.11	1.88	undetermined	82	14.5	3	0.5
247R3_16–18	4	1190.05	Ol-rich troctolite	2.60	2.12	[001]	80	9	10.5	0.5
247R3_19–22	4	1190.08	Ol-rich troctolite	2.69	2.20	[001]	74.5	8	17	0.5
247R3_62–66	4	1190.51	Ol-rich troctolite	5.00	3.81	[010] and [001]	67.5	2	30	0.5
248R2_18–21	4	1193.32	Ol-rich troctolite	2.56	2.03	[001]	77	11.5	11	0.5
248R2_22–24	4	1193.36	Ol-rich troctolite	1.96	1.87	[001]	90	8	1.5	0.5
248R3_33–36	4	1194.82	Ol-rich troctolite	3.45	2.52	[010] and [001]	80	12	7.5	0.5
248R3_36–38	4	1194.85	Ol-rich troctolite	2.44	2.14	[001]	82	14.5	3	0.5
248R3_131–134	4	1195.80	Ol-rich troctolite	2.69	1.81	[010] and [001]	80	10.5	9	0.5
251R1_87–89	4	1207.17	troctolitic gabbro	8.94	-	[001]	40	55	5	0
256R2_83–85	4	1232.27	Ol-rich troctolite	3.04	3.03	undetermined	80	9	10.5	0.5
268R2_83–85	-	1290.06	Ol-gabbro	8.82	5.37	undetermined	10	55	35	0

[a]The spherical harmonic order and Gaussian half width used for in the J index calculations are 22 and 10°, respectively.

2 samples in a second interval from ~552 to 557 mbsf (1 olivine-rich troctolite and 1 olivine gabbro), and 21 samples in a third interval from 1092 to 1196 mbsf (18 olivine-rich troctolites, 1 troctolite, 1 troctolitic gabbro and 1 olivine gabbro) (Table 1 and Figures 1b, 2, and 3).

3. Structures in Olivine-Rich Troctolites and Neighboring Gabbroic Rocks

3.1. Textures and Microstructures

[11] Olivine-rich troctolites are composed of 64%–85% olivine, 2%–24% plagioclase, 1%–30% clinopyroxene, ~1% spinel. Spinel occurs as small subhedral crystals (0.5 mm) with polygonal shape, included in olivine, clinopyroxene or plagioclase. Orthopyroxene oikocrysts are present in one sample (248R2_22–24; Figure 3b). Olivine-rich troctolites are texturally very homogeneous, with large clinopyroxene (5 mm to 1.5 cm) and plagioclase (3 mm to 1 cm) poikiloblasts enclosing coarse-grained subhedral to medium-grained rounded olivine crystals (Figure 3a). In some samples (e.g., 60R3_39–42), clinopyroxene occurs also as interstitial grains with lobate contact against olivine crystals and forms, with plagioclase, pervasive textures (Figure 3f). No shape-preferred orientation marking a visible foliation or lineation was measured in hand samples. The clinopyroxene and plagioclase are always undeformed, with no visible significant distortion/bending of the crystallographic structure. The fine- to medium-grained, rounded olivine chadacrysts are generally devoid of substructures (Figures 3a and 3e). In contrast, coarser grained, subhedral olivine crystals display smooth edges and common, well-defined and widely spaced subgrain boundaries (Figures 3a–3c). Girdles of optically continuous, adjacent grains of subhedral olivine are also observed within clinopyroxene or plagioclase poikiloblasts (Figure 3c). In several samples, a few olivine crystals are slightly elongated, with the long axis generally parallel to [001] axes, and with aspect ratios varying from 1:1.5 to 1:5. The decoration of thin sections by oxidation at 900°C in air [*Kohlstedt et al.*, 1976] commonly reveals free dislocations and dislocation walls in the subhedral olivines (Figure 3d), which indicate plastic deformation by dislocation creep.

[12] Troctolites are composed of 45%–64% olivine, 27%–40% plagioclase, 2%–15% clinopyroxene, and ~1% spinel, which occur as small subhedral grains (0.5 mm) associated with olivine in some samples. Troctolites display an igneous texture, with no foliation observed in our samples. Plagioclase forms large subhedral laths with resorbed grain boundaries (2 to 4 mm) and aspect ratio ranging from 1:1.5 to 1:4. Clinopyroxene, when present, is interstitial to olivine and plagioclase (<1 mm). Plagioclase and clinopyroxene are free of substructure related to crystal plastic deformation. Olivine occurs as aggregates of subhedral, 1 to 4 mm large grains, with well-defined subgrain boundaries (Figure 3g). Most olivines after high-temperature decoration show free dislocations and dislocation walls indicating dislocation creep.

[13] Olivine gabbro is composed of 40%–70% plagioclase, 25%–60% clinopyroxene and more than 5% olivine. In contrast to olivine-rich troctolites and troctolites, spinel is absent in these rocks. Olivine gabbros exhibit an igneous texture, with no foliation observed in our samples. Clinopyroxene grains are large resorbed tablets of 2 mm to 1 cm. Plagioclase, the most abundant phase, occurs as elongated laths or tabular crystals of 1 mm to 1 cm with aspect ratios ranging from 1:1.5 to 1:5. As in troctolite, plagioclase and clinopyroxene do not show evidence of plastic deformation. Olivine occurs as aggregates of subhedral to lobed crystals. Well-defined olivine subgrain boundaries, indicative of crystal plastic deformation, are also observed in olivine gabbros (Figure 3h).

3.2. Crystallographic Preferred Orientations

[14] Olivine, pyroxene and plagioclase CPO of 20 olivine-rich troctolites, 3 troctolites, 1 troctolitic gabbro and 3 olivine gabbros were measured by indexation of electron backscattered diffraction (EBSD) patterns using the SEM-EBSD facility at Geosciences Montpellier. EBSD patterns are generated by interaction of a vertical incident electron beam with a high-quality polished thin section tilted at 70° in a scanning electron microscope JEOL JSM 5600. The diffraction pattern is projected onto a phosphor screen and recorded by a digital CCD camera. This image is then processed and indexed for crystal orientation using the CHANNEL5 software from Oxford Instruments HKL. Crystallographic orientation maps were obtained for each sample, scanning the thin section with a sampling step size ranging from 30 to 80 μm (Figure 4). Indexation rates (fraction of patterns that are automatically indexed during mapping) of the raw maps range from 60% to 85% (Figure 4a). Postacquisition data processing was used to increase the quality of maps by (1) automatically (using a filter that detects pixels having a minimum of 5 neighbors with the

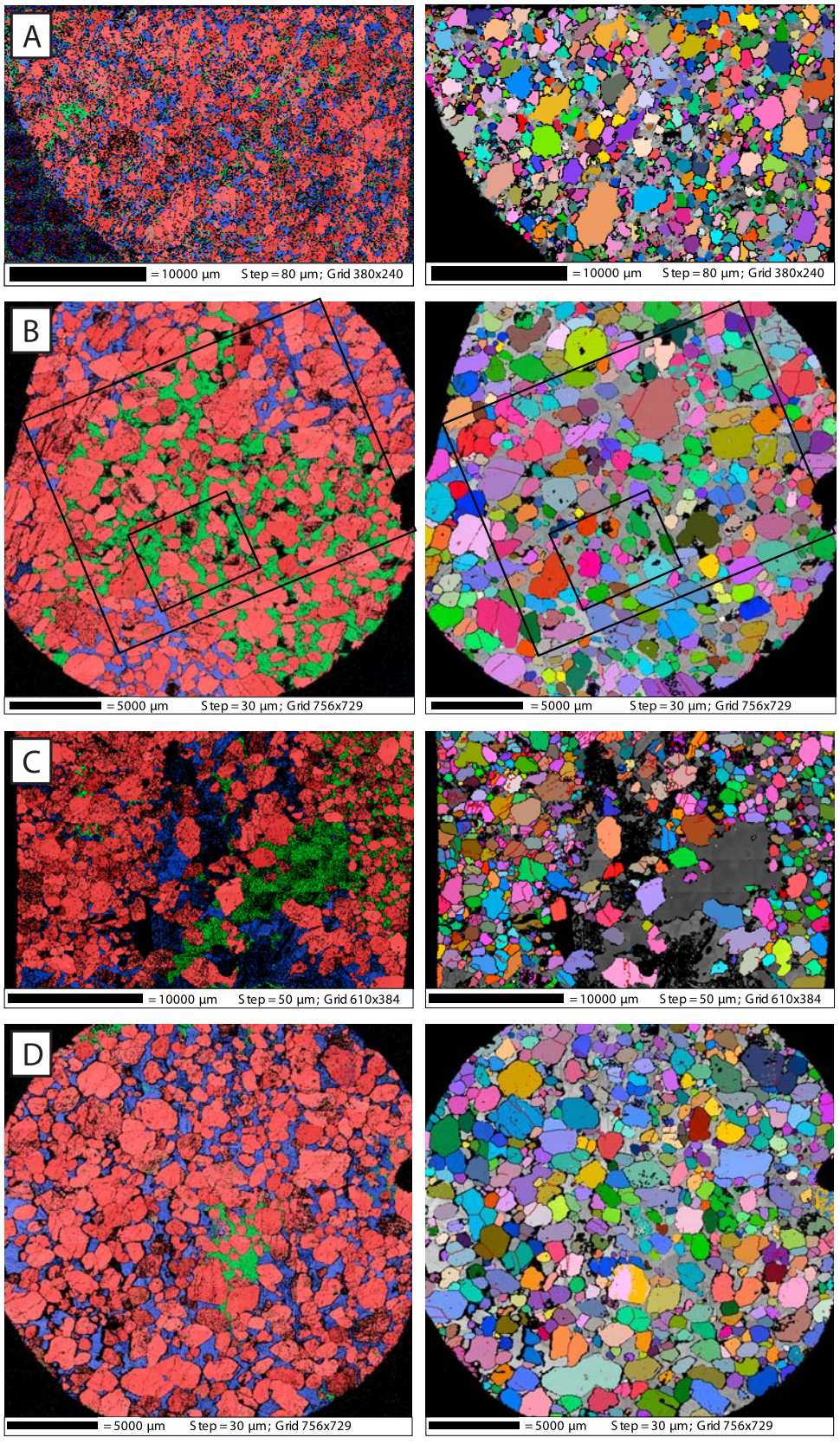
A
= 10000 µm Step = 80 µm; Grid 380x240
= 10000 µm Step = 80 µm; Grid 380x240
B
= 5000 µm Step = 30 µm; Grid 756x729
= 5000 µm Step = 30 µm; Grid 756x729
C
= 10000 µm Step = 50 µm; Grid 610x384
= 10000 µm Step = 50 µm; Grid 610x384
D
= 5000 µm Step = 30 µm; Grid 756x729
= 5000 µm Step = 30 µm; Grid 756x729

Figure 4

same orientation) and manually (when appropriate) filling the nonindexed pixels; (2) identifying the grains, i.e., continuous domains characterized by an internal misorientation <10°; and (3) within each olivine crystal, searching and correcting for systematic indexation errors due to the olivine hexagonal pseudosymmetry, which results in similar diffraction patterns for orientations differing by a 60° rotation around [100]. Pole figures (Figure 5) are presented using the average crystallographic orientation for each grain instead of the raw, gridded data to avoid the overrepresentation of larger grains when the grain size distribution is heterogeneous at the thin section scale. A few samples, mostly in the upper part of the hole, are strongly serpentinized; olivine grains are then poorly indexed, and identification of single grains is consequently difficult resulting in strong biases in the pole figures. Therefore, these samples were excluded and we present the pole figures for a subset of 18 olivine-rich troctolites, 2 troctolites, and 2 olivine gabbros. Only nine of these samples (89R1_92–94, 90R3_8–10, 117R1_55–57, 227R3_124–126, 234R1_27–29, 247R3_16–18; 248R2_22–24; 248R3_36–38; 256R2_83–85) were oriented in the core reference frame (Figure 5).

[15] Olivine CPOs in olivine-rich troctolites are very weak, with fabric strength (J index; [*Bunge*, 1982; *Ben Ismail and Mainprice*, 1998]) values ranging from 1.6 to 3.8 (Table 1). Nevertheless, CPO patterns are not random but remarkably consistent (Figure 5); they are characterized by [100] being generally the more scattered axis, a [010] concentration that possibly correspond to the pole to the foliation, and a relatively stronger, unusual [001] point or girdle cluster. The analysis of Misorientation Angle Distributions (MAD) of correlated (neighbor pairs) gridded data points gives indications on the misorientation axis of subgrain boundaries, and therefore on the active slip system(s) during deformation (Figure 6). In most samples, the MAD of correlated data points show a peak at low misorientation angles (2 to ~15–20°), with a higher amplitude than predicted by the theoretical random distribution. This is consistent with the occurrence of subgrains and adjacent grains derived from subgrains. The dominant associated rotation axis is close to [001] in most samples as indicated by the inverse pole figures of misorientation axes (Figures 6a–6d and Table 1); this indicates that olivine crystal plastic deformation is related to dislocation creep with activation of the dominant (010) [100] slip system, one of the most commonly observed, and the easiest slip system in mantle peridotites [e.g., *Durham and Goetze*, 1977; *Durham et al.*, 1977; *Ben Ismail and Mainprice*, 1998; *Tommasi et al.*, 2000]. This analysis is confirmed by observations made on EBSD maps (Figure 4): we manually checked the maps for the subgrain rotation axes using misorientation profiles across subgrain boundaries when present (red lines in olivine crystals in Figure 4), which dominantly appear to be (100), or close to (100). [010] is a less common, but also identified rotation axis for low-angle misorientations (Figure 6), likely indicating activation of the (001)[100] slip system which is also commonly active, but less easy in natural peridotites at high temperature [e.g., *Tommasi et al.*, 2000]. In most natural peridotites deformed in asthenospheric conditions, CPOs result from the dominant joint activity of both the (010)[100], and (001)[100] slip systems [*Tommasi et al.*, 2000]. In some samples (Figures 6b and 6c), [100] seems to be also a preferred (but minor) rotation axis for misorientation, which may reveal the activity of (010)[001] (also active at high temperature in olivine) and/or the occurrence of screw dislocations in the dislocation walls.

[16] Olivines in troctolites have weak, random CPO (Table 1), as illustrated by the two examples in Figure 5. The MAD analysis also shows a relatively high density of low misorientation angles, mainly characterized by rotation axes close to [010] and [001], which is consistent with the joint activity of (010)[100] and (001)[100] at high temperature in olivine (Figure 6e). Plagioclase and clinopyroxene do not show any significant CPO.

[17] Olivine CPO in olivine gabbros are generally stronger than in olivine-rich troctolites and troctolites (Table 1), but with no clear, distinctive patterns (Figure 5), which may be a measurement artifact due to the relatively low number of measured grains [e.g., *Ben Ismail and Mainprice*, 1998]. The lack of easily identifiable CPO pattern can also

Figure 4. EBSD maps of olivine-rich troctolites. (a) Sample 233R3_21–24. (b) Sample 247R3_16–18. The large and small rectangles indicate the localizations of the microphotographs in Figures 3a and 3e, respectively. (c) Sample 248R2_18–21 (from the core pictured in Figure 2c). (d) Sample 248R3_36–38. (left) Raw maps. Each color corresponds to one mineralogical phase: red, olivine; blue, plagioclase; green, clinopyroxene; black, no results (i.e., no mineral, or nonindexed mineral). (right) Processed map for olivine (see section 3.2 for further explanations on data processing). The color is a function of crystal orientation generated using the "all euler" function in HKL software. Red lines in olivine grains indicate subgrain boundaries (misorientation <10°).

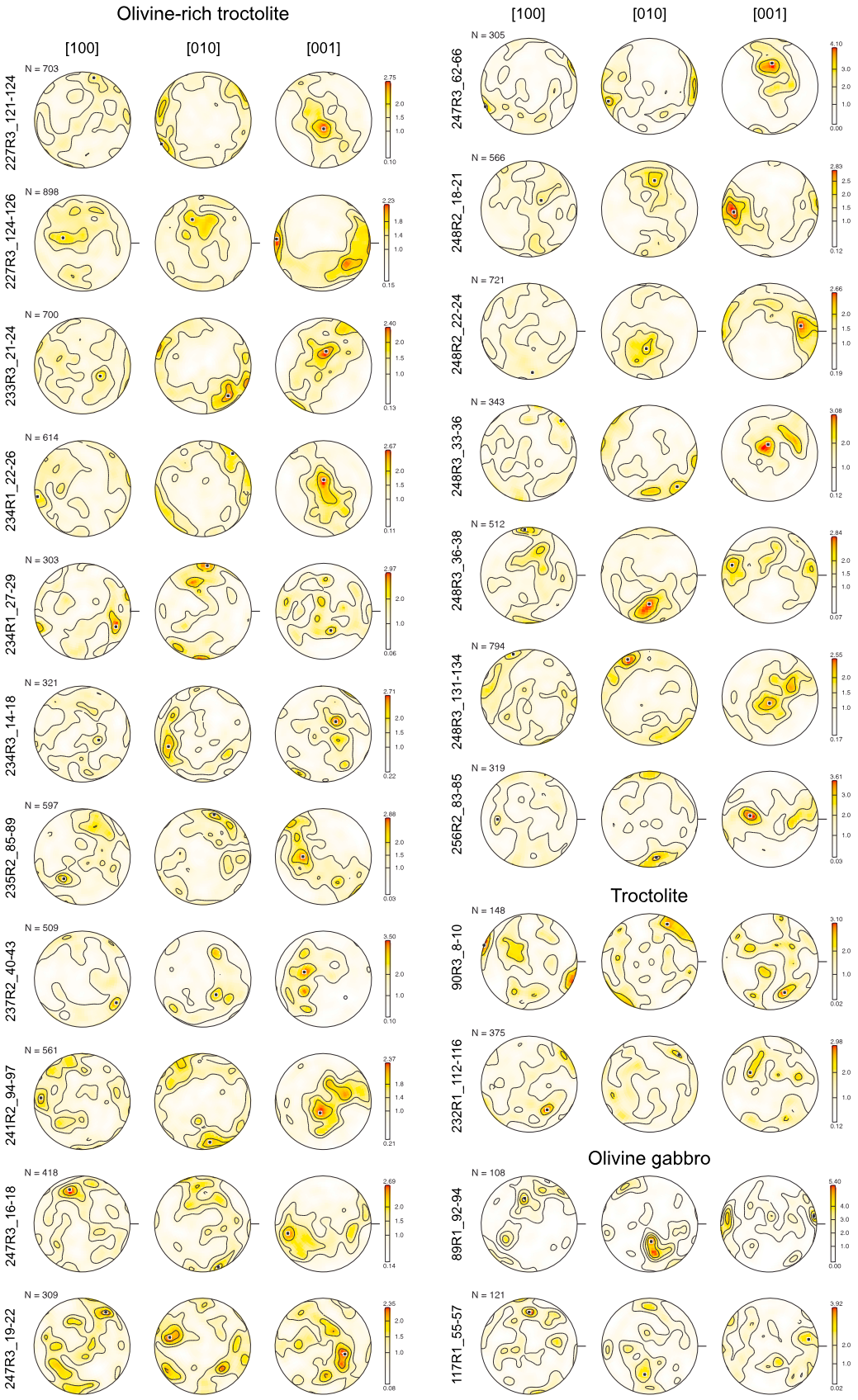
Olivine-rich troctolite
[100]
[010]
[001]
227R3_121-124
N = 703
227R3_124-126
N = 898
233R3_21-24
N = 700
234R1_22-26
N = 614
234R1_27-29
N = 303
234R3_14-18
N = 321
235R2_85-89
N = 597
237R2_40-43
N = 509
241R2_94-97
N = 561
247R3_16-18
N = 418
247R3_19-22
N = 309
247R3_62-66
N = 305
248R2_18-21
N = 566
248R2_22-24
N = 721
248R3_33-36
N = 343
248R3_36-38
N = 512
248R3_131-134
N = 794
256R2_83-85
N = 319
Troctolite
90R3_8-10
N = 148
232R1_112-116
N = 375
Olivine gabbro
89R1_92-94
N = 108
117R1_55-57
N = 121

Figure 5

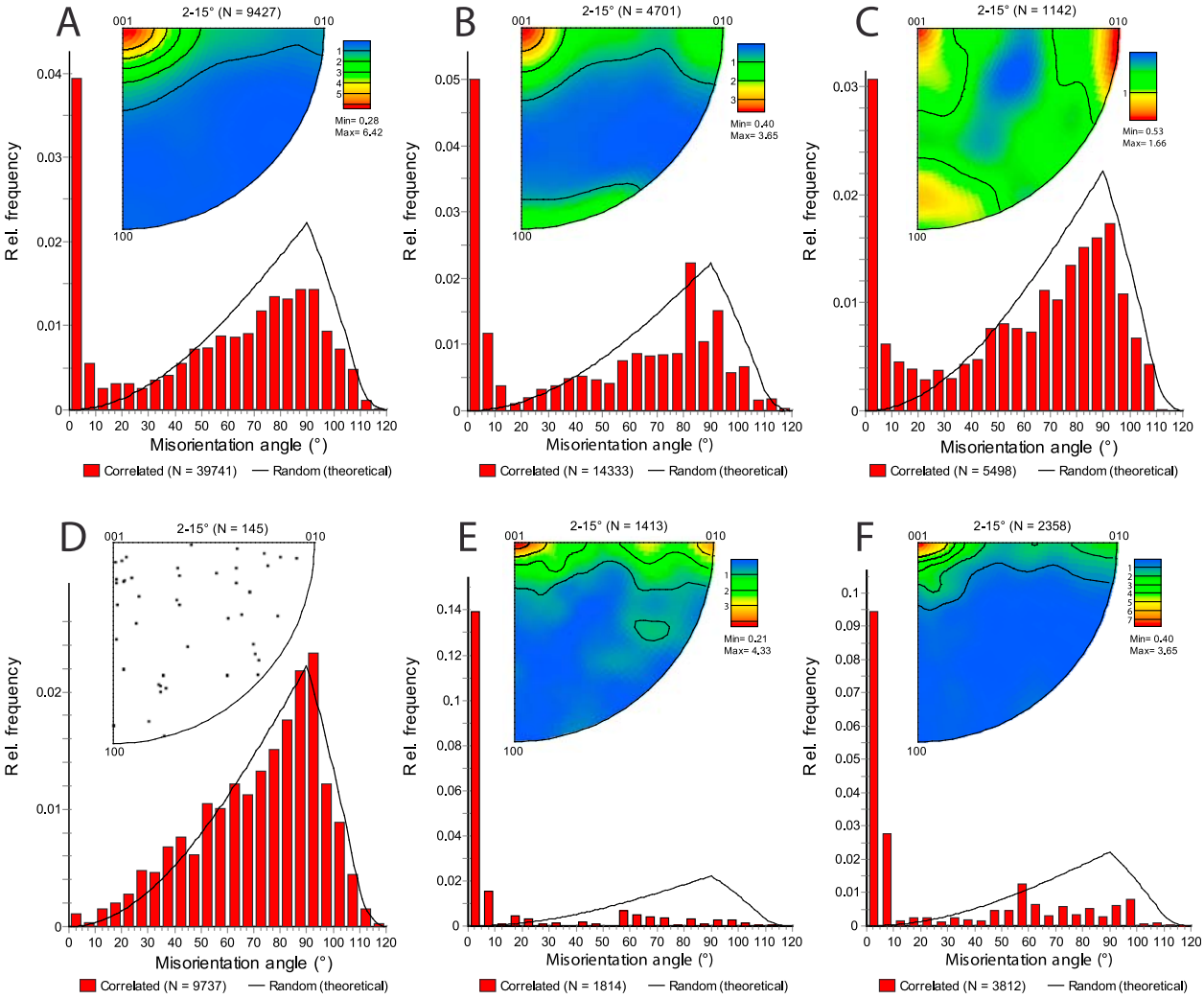

Figure 6. Misorientation angle distribution (MAD) and rotation axes for the low (2–15°) misorientation angles in the crystal reference frame, in (a–d) olivine-rich troctolite, (e) troctolite, and (f) olivine gabbro samples. Figure 6a shows sample 248R2_22–24, Figure 6b shows sample 247R3_16–18, Figure 6c shows sample 227R3_121–124, Figure 6d shows sample 233R3_21–24, Figure 6e shows sample 70R2_99–103, and Figure 6f shows sample 117R1_55–57. MAD histograms present data for correlated points (angle between neighbor measurement points) compared to the theoretical random distribution. Contours in the inverse pole figures are × multiple of uniform distribution. N is number of measurement points for each diagram.

result from the relatively low olivine abundance in olivine gabbro, the deformation of each isolated olivine grain being then possibly slightly different rather than recording an homogenous strain field at the sample scale. The analysis of MAD (Figure 6f) reveals patterns similar to those seen in troctolites, consistent with observed well-developed (100) subgrain boundaries in olivines, and with dislocation creep dominantly involving (010) [100] and (001) [100] slip. Plagioclase and clinopyroxene are not deformed.

4. Discussion

[18] In olivine-rich troctolites, clinopyroxene and plagioclase poikiloblasts are not deformed, while the olivine chadacrysts show evidence of high-

Figure 5. Olivine crystallographic preferred orientations (CPO) in olivine-rich troctolites, troctolites, and olivine gabbros. Equal-area, lower hemisphere stereographic projections; N is the number of measured grains; and contours are × multiple of uniform distribution. The small black squares indicate the orientation of the maximum intensity in the pole figures. A small tick mark on the right side of some pole figures indicates the top of the core for oriented samples.

temperature plastic deformation by dislocation creep. In addition, clinopyroxene and plagioclase crystallized after the same MORB melt that was in chemical disequilibrium with the partly corroded olivine [*Drouin et al.*, 2009]. These observations preclude a common magmatic origin for clinopyroxene, plagioclase and olivine, and imply that plastic flow predates the crystallization of the melt. They suggest a complex magmatic history with percolation and crystallization of a MORB-type melt within a preexisting, previously deformed olivine-rich matrix, with high rates of melt renewal, and the joint crystallization of plagioclase and clinopyroxene before reaching complete equilibration between melt and the corroded olivine grains [*Drouin et al.*, 2009]. However, the origin of the preimpregnation olivine matrix remains ambiguous, and difficult to constrain. It could represent an earlier, very primitive cumulate plastically deformed at the base of the lithosphere, or it could derive from mantle peridotite, as speculated by *Drouin et al.* [2009] based on the in situ geochemical arguments.

[19] In sections 4.1–4.3, we discuss the potential effects of melt-rock interactions on the development of olivine CPOs, the different possible origins of olivine-rich troctolites, and the implications of the occurrence of the olivine-rich troctolites on accretion processes at slow spreading ridges.

4.1. Olivine CPO in Olivine-Rich Troctolite: Typical of Melt Impregnation?

[20] The observed olivine microstructures in olivine-rich troctolites suggest that olivine deformation was accommodated by dislocation creep at high temperature, with activation of the main slip systems (010)[100], (001)[100], and to a minor extent (010)[001], which are most commonly described in mantle peridotites as a result of asthenospheric flow [e.g., *Tommasi et al.*, 2000]. However, olivine CPOs are particularly weak, and most samples display a maximum concentration of [001]. Such CPOs are not commonly described in mantle peridotites [*Ben Ismail and Mainprice*, 1998; *Tommasi et al.*, 2000]; a [001] preferred orientation is not consistent with the high-temperature (010)[100] and (001)[001] slip systems, which normally results in strong [100] clusters parallel to the lineation. Nevertheless, weak olivine CPOs with a tendency for a stronger [001] maximum have been measured in zones of melt accumulation and impregnation (Figure 7), such as the mantle/crust transition zone in the Oman ophiolite [*Ceuleneer and Rabinowicz*, 1992; *Boudier and Nicolas*, 1995; *Jousselin et al.*, 1998; *Dijkstra et al.*, 2002], or the Kondyor ultramafic complex [*Burg et al.*, 2009]. *Nicolas and Prinzhofer* [1983], and *Boudier and Nicolas* [1995] proposed that the weaker olivine CPOs in wehrlite and impregnated dunite could result from the desegregation, by large volumes of magma, of an olivine-rich matrix; olivine grains are dispersed in impregnating melt and loose their original fabric.

[21] We commonly observe in our samples girdles of subhedral olivine grains that show limited misorientation between each other, with (100) subgrain boundaries and curviplanar grain boundaries (Figures 3c and 3e). Interstitial spaces between boundaries of adjacent olivines crystals are filled by clinopyroxene or plagioclase. We postulate that corrosion of olivine grains is easier along grain boundaries, as well as along dislocation walls (subgrain boundaries have higher vacancy concentration than the olivine structure, and are interfaces that are structurally close to grain boundaries [e.g., *Sutton and Balluffi*, 1995]). Hence melt may have preferentially corroded olivine grains along (100) subgrain boundaries to form girdles of new grains with smooth edges [*Donaldson*, 1985; *Boudier*, 1991]. This is also supported by the observation of adjacent olivine crystals, enclosed in clinopyroxene or plagioclase, which share the same optical orientation, suggesting that they derive from a single crystal (e.g., Figure 3a). We interpret the dispersed, undeformed, and smaller rounded olivines that occur isolated in large clinopyroxene and plagioclase oikocrysts (Figures 3a and 3e) as the end product of such a corrosion/dissolution process. The lack of free dislocations in the smallest rounded olivine crystals, observed in decorated thin sections, could be indicative of melt-assisted annealing.

[22] Alternatively, the small, rounded grains could represent crystals directly crystallized from the impregnating melt, thus never deformed. However, we discard this interpretation because (1) the crystallographic orientation of these small olivine grains is commonly close to neighboring larger olivine grains that commonly display subgrain boundaries (Figure 3a) and (2) they are not in chemical equilibrium with the surrounding clinopyroxene and/or plagioclase [*Drouin et al.*, 2009]. We propose that extensive impregnation by melt has significantly modified the style of the original olivine CPO. In a first stage, the olivine-rich matrix was plastically deformed, producing fabrics as a result of dislocation creep, which seems to be dominated by the most common and easy (010)[100] slip system. Then, melts infiltrated the olivine matrix via crystal corrosion along grain and subgrain boundaries, and, as

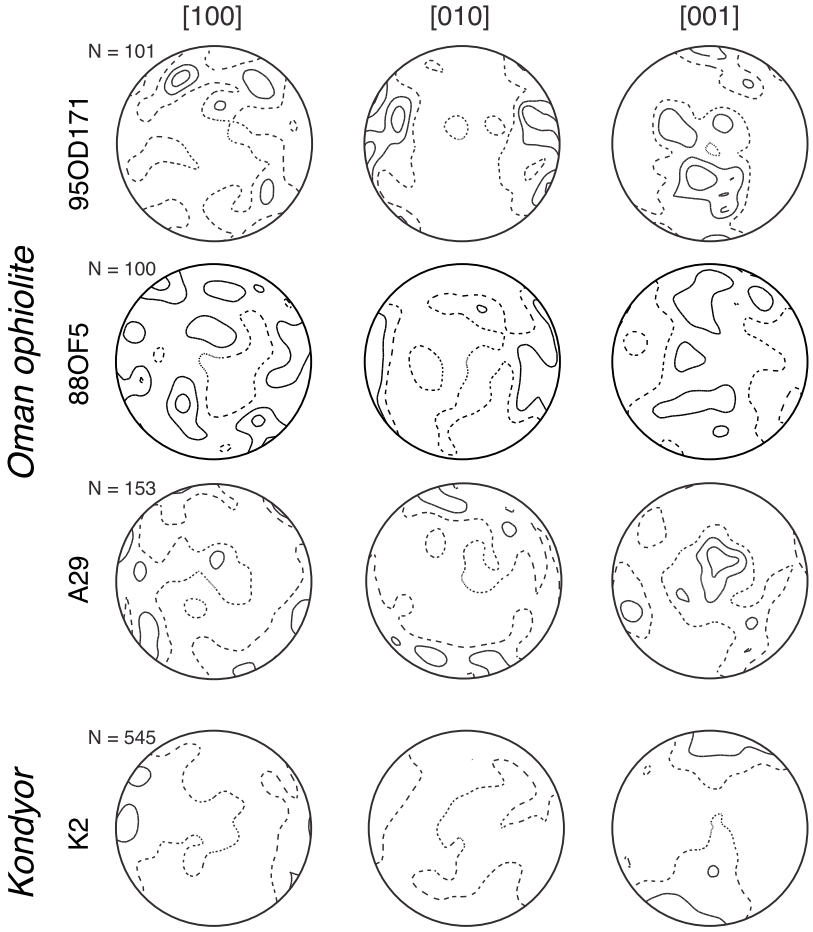

Figure 7. Compilation of previously published CPOs in impregnated peridotites. The three samples from the Oman ophiolites are located in the mantle/crust transition zone or at the base of the layered gabbro section and are described as impregnated dunite (95OD171 [*Jousselin et al.*, 1998]), wherlite intrusive in the lower layered gabbro (88OF5 [*Boudier and Nicolas*, 1995]), and wehrlite showing poikilitic clinopyroxene and plagioclase (A29 [*Dijkstra et al.*, 2002]). The K2 sample from the Kondyor mantle diapir is a wehrlite [*Burg et al.*, 2009]. Contours correspond to x times the uniform distribution, with x = 1 for the dashed contour and a contour interval of 1; N is number of measured grains.

the melt fraction increased, crystals became free to move, with slight rotations relative to each other inducing a dispersion of the preexisting olivine CPO [e.g., *Cannat et al.*, 1990]. We thus interpret the weakness of the measured fabrics as partly resulting from melt-assisted dispersion of a preexisting fabric, which intensity is unknown but was not necessarily weak. This effect may add to another CPO weakening mechanism, which is the process of dunitization in the case of a mantle protolith [*Tommasi et al.*, 2004] (see section 4.2). The unusual clustering of [001] axes in the measured CPOs then results from the process outlined above: corrosion and division of preexisting olivine grains, preferentially along (100) subgrain boundaries (e.g., Figure 3c), followed by misorientation of newly formed grains by small rotations preferentially around [001] [*Poirier and Nicolas*, 1975] when the melt fraction is high enough to destroy the solid framework. Disruption of the solid olivine framework may happen locally, and/or episodically during the overall impregnation history recorded by the rock. This implies that, at least during part of this process, the melt influx within the solid matrix is high enough to allow crystallization of relatively large amounts of clinopyroxene and/or plagioclase with constant and uniform chemistry, as documented by *Drouin et al.* [2009].

[23] The clustering of [001] could in principle be enhanced by suspension flow of olivine grains (with [001] being the longest axis when elongated), which requires that the melt fraction locally exceeds

~30% [e.g., *Van der Molen and Paterson*, 1979; *Vigneresse et al.*, 1996; *Rosenberg and Handy*, 2005] to allow the transition from solid-state, plastic flow to local suspension flow to occur. However, no significant shape fabric was observed in our samples, and the effect of suspension flow can only be limited here. We anticipate that the proposed mechanism for producing the observed uncommon CPOs (i.e., preferred rotation of grains around [001] following corrosion and disruption of the solid olivine framework) does not require significant amount of magmatic flow.

[24] High-temperature plastic deformation of olivine is also described in Hole U1309D gabbro samples studied herein. Oceanic and ophiolitic gabbros commonly exhibit CPOs and subgrain microstructures in olivine crystals while there is no or little evidence for dislocation creep in coexisting plagioclase and pyroxene [e.g., *Boudier et al.*, 1996; *Dick et al.*, 1999; *Yoshinobu and Hirth*, 2002]. At hypersolidus conditions, the olivine is the weakest phase, and easily records small amounts of intracrystalline plastic deformation in a crystal-rich mush [*Yoshinobu and Hirth*, 2002]. However, the CPOs measured in olivine-rich troctolites are inconsistent with high-temperature creep of an olivine framework in a crystal-rich mush; in this scenario, the inferred (010)[100] slip system should produce a high-temperature CPO dominated by the preferred alignment of [100], even if the recorded finite strain was weak.

4.2. Are Olivine-Rich Troctolites Primitive Cumulates or the Ultimate Product of Melt-Mantle Interactions?

[25] Olivine-rich rocks, largely observed in ophiolite mantle/crust transition zones, are generally absent in gabbro suites sampled at slow and ultraslow spreading ridges [e.g., *Dick*, 1989; *Kelemen et al.*, 2007]; yet, the occurrence of these primitive cumulates is required to balance the MORB composition observed at the surface. [e.g., *Dick et al.*, 2000; *Coogan et al.*, 2001; *Coogan*, 2007; *Kelemen et al.*, 2007]. Olivine-rich troctolites are observed as discrete intervals, a few meters thick, intercalated with olivine and troctolitic gabbros intervals within the site U1309 gabbroic sequence. Because of their relative abundance (~5%) and of their primitive bulk composition [*Blackman et al.*, 2006; *Godard et al.*, 2009], these rocks were obvious candidates for being the "missing" cumulates, characterizing the, unsampled yet, most primitive portions of the lower oceanic crust. In this scenario, the olivine-rich matrix in the olivine-rich troctolites would correspond to the earliest product of the differentiation of MORB parental melts. These primitive cumulates would have then recorded some high-temperature plastic deformation at the base of the lithosphere before being impregnated, in a second magmatic stage, by less primitive MORB melts. The latter could also form associated gabbroic rocks, which are made of clinopyroxene and plagioclase with the same trace element composition than in olivine-rich troctolites [*Drouin et al.*, 2009]. However, the composition of olivine in olivine-rich troctolites (highly fractionated trace element patterns with a strong depletion in light rare earth elements and other highly incompatible elements) is not consistent with a formation by simple fractionation after MORB-type melts [*Drouin et al.*, 2009].

[26] An alternative to a cumulate origin for the olivine in olivine-rich troctolites is a mantle origin. In addition to the similarities of the CPOs with impregnated peridotite CPOs pointed out in section 4.1 (Figure 7), olivine-rich troctolites display poikilitic textures that are very similar to the impregnation textures commonly described in the shallow mantle sampled at fast spreading ridges [e.g., *Cannat et al.*, 1990; *Constantin et al.*, 1995; *Allan and Dick*, 1996; *Arai and Matsukage*, 1996; *Dick and Natland*, 1996; *Niu and Hekinian*, 1997]. Both ultramafic cumulates and mantle rocks, when impregnated by large volumes of basaltic melts, would have similar textures and major element composition of minerals. In the case of impregnated mantle peridotites, elements having high diffusion coefficients in high-temperature magmatic systems, such as Fe and Mg [e.g., *Chakraborty*, 1997], reequilibrate rapidly in melts and in the percolated silicate framework. As a result, residual olivine will lose its original mantle composition (i.e., low Ni and Mg contents compared to typical mantle olivine). Trace elements are generally thought to have lower diffusion coefficients in silicates under the same thermodynamic conditions, which would explain the contrasting results obtained in olivine-rich troctolites: complete equilibrium between silicate phase for Mg-Fe and, apparently, strong disequilibrium between olivine and associated clinopyroxene and plagioclase [*Drouin et al.*, 2009]. However, data on diffusion coefficients of trace element in olivine are too scarce and contradictory [*Spandler et al.*, 2007; *Cherniak*, 2007] to allow a definite characterization and quantification of these reequilibration processes today.

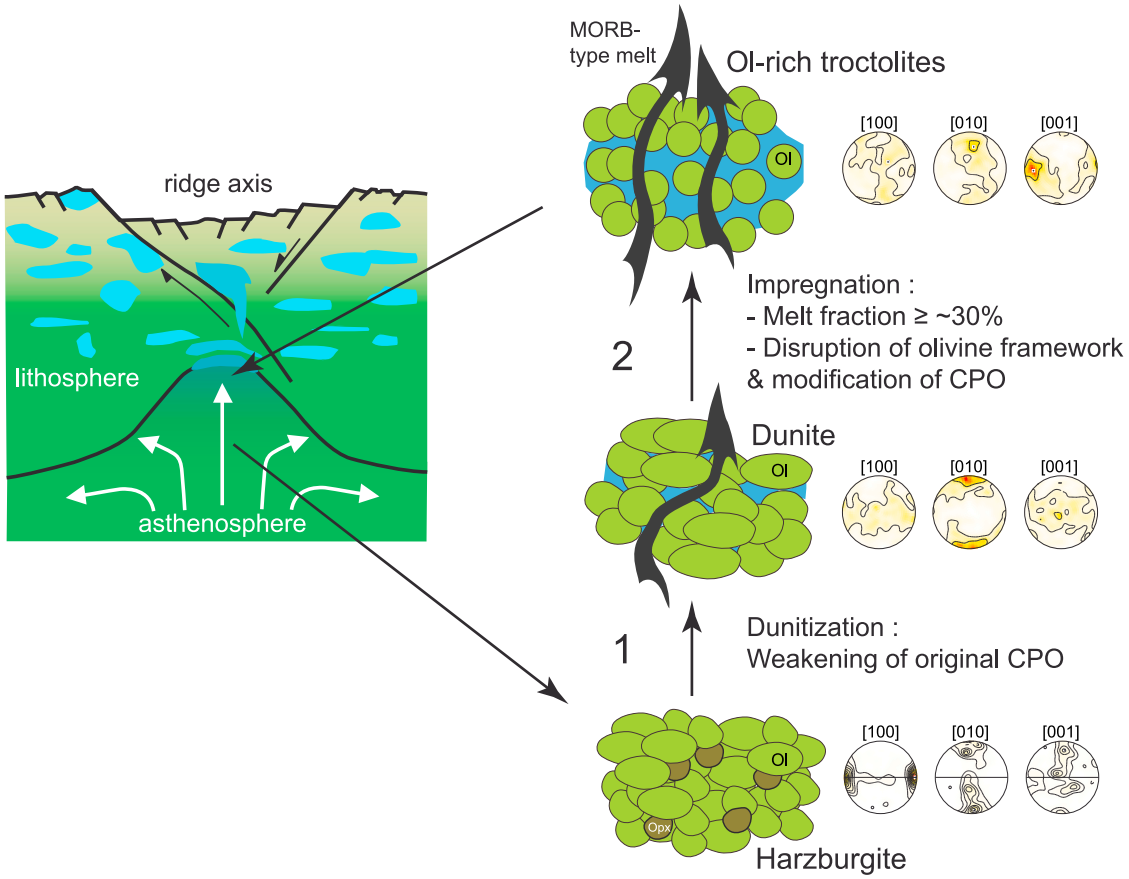

Figure 8. Sketch of the proposed scenario for the formation of Hole U1309D olivine-rich troctolites. Percolation of basaltic melts through depleted mantle peridotite at near solidus temperature results in dunitization (orthopyroxene dissolution, precipitation of olivine, and formation of dunite), with weakening of olivine CPO (indicated by 1), and impregnation when increasing melt fraction (≥30%) locally disrupts the olivine framework and further modifies the olivine CPO (indicated by 2). The dunitization and impregnation are viewed as successive stages of a continuous process. As temperature decreases, melt crystallizes plagioclase and clinopyroxene within the assimilated olivine matrix to form olivine-rich troctolite. The schematic cross section of the ridge axis is modified from *Cannat* [1996]. The examples of original harzburgite and dunite CPOs are from Polynesian xenoliths (RPA18A and UAH280X, respectively [*Tommasi et al.*, 2004]). Note the absence of structural reference frame (no visible foliation in samples) for the dunite and olivine-rich troctolite CPOs.

[27] Because of their microstructural and textural similarities with impregnated peridotites from ophiolites and present-day mid-ocean ridges, we posit a mantle origin for the olivine-rich troctolites sampled at Site U1309D, although no single unequivocal criterion allows characterizing conclusively the origin of the olivine in these rocks yet. The olivine-rich troctolite intervals are relatively small units, in which no relict of the preimpregnation lithology can be observed, and no gradient of the amount of impregnation is observed. An additional reason for favoring the mantle origin is the weakness of the olivine CPO; in the upper mantle, impregnation would likely be preceded by dunitization, which is an efficient mechanism to significantly weaken the original olivine CPO, as illustrated by the study of Polynesian xenoliths by *Tommasi et al.* [2004].

[28] We propose the following scenario for the formation of Hole U1309D olivine-rich troctolites (Figure 8):

[29] 1. In the first stage, MORB melts are sporadically injected into the molten depleted mantle at near solidus temperature. High temperature favors pervasive melt-rock interactions, orthopyroxene dissolution and dunitization [e.g., *Kelemen*, 1990; *Kelemen et al.*, 1990; *Niu*, 2004; *Tommasi et al.*, 2004]. This stage of reactive melt percolation can

largely contribute to the reduction of the strength of the high-temperature crystallographic preferred orientation [*Tommasi et al.*, 2004]. Should a cumulate origin be favored for the olivine, this first stage can be replaced by the near complete crystallization of a primitive cumulate. These two possible origins are actually not necessarily exclusive.

[30] 2. The olivine-rich solid matrix is progressively impregnated by melt; melt accumulates, corrodes preexisting olivine grains, and the melt fraction becomes locally sufficiently large to disaggregate the olivine framework, further weaken the fabric and reinforce the clustering of [001]. This second stage postdates olivine plastic deformation and dunitization. We see no significant variability in the final CPO style that could potentially be related to variable extents of melt impregnation at the scale of the olivine-rich troctolite intervals; CPOs are consistently weak and generally display a slightly stronger [001]. The same microstructural scenario is proposed for wherlites from the periphery of the Kondyor translithospheric diapir in Russia [*Burg et al.*, 2009], in which the olivine CPO shows a similar peculiar [001] concentration in an overall weak fabric (Figure 7).

[31] 3. In the third stage, as temperature decreases, melt progressively crystallizes plagioclase and clinopyroxene within/around the assimilated olivine matrix [*Drouin et al.*, 2009] to form the olivine-rich troctolite.

[32] The gabbroic section that was sampled in IODP Hole U1309D was built by multiple, relatively small intrusive events at different depths in the axial lithosphere [*Blackman et al.*, 2006; *Grimes et al.*, 2008; *Godard et al.*, 2009; D. K. Blackman et al., Drilling constraints on lithospheric accretion and evolution at Atlantis Massif, Mid-Atlantic Ridge 30°N, submitted to *Journal of Geophysical Research*, 2010]. Narrow intervals of impregnated peridotites were sampled at the top of Hole U1309D [*Blackman et al.*, 2006; *Tamura et al.*, 2008; *Godard et al.*, 2009] indicating that small slivers of mantle can be trapped within the gabbroic intrusions. We regard olivine-rich troctolites as representing similar slivers (maximum thickness is ~12 m) of heavily impregnated mantle (or possibly early primitive cumulates). The occurrence in the recovered gabbroic sequence of ultramafic rocks that have undergone extensive melt/rock interactions suggests that melt percolation and impregnation occurred in hot lithosphere, probably at the asthenosphere/lithosphere transition.

4.3. Implications for Accretion Processes at Slow Spreading Ridges

[33] The formation of the olivine-rich troctolites recovered in the IODP Hole U1309D gabbroic section is associated with abundant melt accumulation and impregnation at the base of the lithosphere beneath the ridge axis in this area of the Mid-Atlantic ridge. The association of troctolites and olivine gabbros with impregnated olivine-rich rocks in Hole U1309D is similar to what has been documented in fast spreading mantle-crust transition zones in the Oman ophiolite [e.g., *Boudier and Nicolas*, 1995; *Dijkstra et al.*, 2003] and at Hess Deep [*Allan and Dick*, 1996; *Arai and Matsukage*, 1996; *Dick and Natland*, 1996]. However, in contrast to fast spreading environments, the crust at 30°N is poor in volcanics, classically considered as "magma-poor," and accretion is dominated by detachment faulting [*Cann et al.*, 1997; *Blackman et al.*, 2002].

[34] Our results, together with the abundance of igneous rocks in Hole U1309D [*Blackman et al.*, 2006], demonstrates that magmatic activity, at the time of the formation of the gabbroic sequence that now constitutes the core of the Atlantis Massif, was relatively high. This is in apparent contradiction with the paucity of erupted basalts, the occurrence of outcropping mantle peridotites on the seafloor in this area, and with the traditional view that OCC formation is related to waning magmatic activity [e.g., *Tucholke and Lin*, 1994]. It suggests that most of the melt that produced the recovered crustal section remained trapped in the lithosphere [e.g., *MacLeod et al.*, 2009], with no or little erupted volcanic counterpart, resulting in a composite crust made of gabbroic plutons embedded in peridotites at depth or serpentinites closer to the seafloor and a reduced or locally absent basaltic upper crust, as already described at the mid-Atlantic and Southwest Indian Ridges [e.g., *Cannat*, 1993; *Cannat et al.*, 1995; *Lagabrielle et al.*, 1998; *Cannat et al.*, 2006; *Dick et al.*, 2006], and in Alpine ophiolites [e.g., *Lagabrielle and Cannat*, 1990]. This interpretation is supported by the overall geochemical signature of IODP Hole U1309D [*Godard et al.*, 2009], and is consistent with the discrepancy between crustal thicknesses inferred from gravimetry and from melting models [*Escartín and Cannat*, 1999; *Cannat et al.*, 2004]. It is also consistent with thermal modeling [*Sleep and Barth*, 1997], and with the results of *Lizarralde et al.* [2004] who propose from seismic refraction and gravimetry data that,

at spreading rates below 20 mm/yr, significant amounts of melt might be retained in the mantle.

[35] Extending our results to all volcanic-poor areas, where accretion is dominated by detachment faulting, and which could represent as much as 50% of slow spreading ridges [*Escartín et al.*, 2008], we speculate that incorporation of impregnated ultramafic rocks, possibly mantle peridotites, to gabbroic sections is a widespread, and fundamental way of building the lower crust at slow and ultraslow spreading ridges. OCCs, which are a subset of detachment fault systems at slow and ultraslow spreading ridges, represent a relatively magma-rich end-member of composite crust. Several recent studies, using independent arguments (gravimetry and bathymetry analysis, ocean drilling results) demonstrate that OCCs develop during or immediately after episodes of relatively high magma supply and do not represent the magma-starved end-member of accretion processes at mid-ocean ridges [*Cannat et al.*, 2006; *Ildefonse et al.*, 2007; *Blackman et al.*, 2008; *Tucholke et al.*, 2008]. *Ildefonse et al.* [2007] have proposed that fully developed OCCs such as the Atlantis massif are the morphological expression of the occurrence of larger than usual, discrete gabbroic plutons in a composite crust, corresponding to episodically enhanced magmatic activity.

[36] Based on the proposed scenario for the formation of the olivine-rich troctolite, we can speculate on the possible episodic occurrence of relatively melt-rich lenses, or sills in the upper asthenospheric mantle or at the lithosphere/asthenosphere boundary in volcanic-poor regions of slow spreading ridges. Considering the thickness of the olivine-rich troctolites units recovered in Hole U1309D, these sills may be thick enough (ten to several tens of meters?) to be detected seismically with appropriately designed seismic experiments. However, one additional difficulty, compared to fast spreading ridges, is that such melt-rich lenses are expected to be transient, and possibly as deep as 15–20 km if we consider the largest inferred crystallization depth of troctolitic rocks in comparable settings [*Kelemen et al.*, 2007].

[37] The melt-rock interactions that are associated to the formation of melt-rich lenses of impregnated ultramafic material are expected to modify significantly the geochemical signature of percolating melts (e.g., enrichment in MgO, and relative depletion in CaO and Al_2O_3). Hence, in a way similar to the primitive cumulates described by *Lissenberg and Dick* [2008], the olivine-rich troctolite studied herein represents another piece of the petrogeochemical puzzle that is necessary to document in order to ultimately link the geochemistry of MORB to mantle melting processes.

5. Conclusion

[38] Together with their in situ mineral compositions [*Drouin et al.*, 2009], the microstructures of olivine-rich troctolites from IODP Hole U1309D suggest that high degrees of melt impregnation contributed to their final texture, chemistry and microstructure. The observed olivine substructures and misorientations are consistent with deformation by dislocation creep, dominated by the main high-temperature (010)[100] and (001)[100] slip systems, as commonly described in mantle peridotites.

[39] The measured CPOs differ from classical mantle fabrics in that they are much weaker, with slightly stronger [001] clusters. We interpret these fabrics as recording the last stages of extensive melt impregnation of a previously deformed olivine-rich rock, with separation of olivine grains by preferred corrosion along grain boundaries and (100) subgrain boundaries. Melt impregnation is recorded by the rock texture, with the crystallization of poikilitic and interstitial pyroxene and plagioclase and corrosion of olivine that postdate olivine deformation, and by crystal chemistry [*Drouin et al.*, 2009].

[40] Similar textures and CPO are observed in the mantle/transition zone of ophiolites. Based on this similarity, we propose that olivine in olivine-rich troctolites is derived from mantle peridotites. In this scheme, olivine-rich troctolites represent the ultimate product of a multistage melt-mantle reaction process, in which dunitization contribute to weaken the CPO, prior to the impregnation and disruption of the olivine framework. The mantle origin of olivine, though, is not demonstrated unequivocally in this study; the protolith of the olivine-rich troctolites could be either mantle peridotite, or a primitive cumulate, or a combination of both. In any case, it must be emphasized that melt impregnation primarily controls the chemistry and microstructure of olivine-rich troctolites, and implies large melt fluxes at the base of the lithosphere.

[41] The occurrence of a significant volume of olivine-rich troctolites in IODP Hole U1309D suggests that magmatic activity at the ridge axis was high when the recovered crustal section was emplaced. This is consistent with the already stated hypotheses, inferred from several, independent constraints, that melt production in volcanic-poor

areas of slow spreading ridges is not necessarily low, and that the development of OCCs is associated to relatively rich magmatic episodes in an overall composite crust. The olivine-rich troctolites were recovered as relatively thin (<12 m), discrete intervals, which we speculate to represent relatively small slivers of impregnated ultramafic rocks, trapped in a stack of small gabbro intrusions. Extending this accretion mode to the entire portion of the mid-ocean ridge that is accreted through detachment faults, it may represent an essential piece of the lithosphere accretion puzzle at ultraslow and slow spreading ridges. The contribution of melt-rock interactions that control the formation of olivine-rich troctolites to MORB geochemistry is expected to be significant at slow spreading ridges.

Acknowledgments

[42] This research used samples and data provided by the Integrated Ocean Drilling Program (IODP). We thank captains Pete Mowat and Alex Simpson; the operation superintendents Mike Storms, Stephen Midgley, and Ron Grout; the crew of the *JOIDES Resolution*; and the Integrated Ocean Drilling Program United States Implementing Organization's technical staff for their outstanding work during IODP Expeditions 304 and 305. We are grateful to Christophe Nevado and Doriane Delmas for providing high-quality thin sections. We also thank F. Boudier, A. Tommasi, D. Mainprice, and G. Hirth for stimulating discussions. The manuscript benefited from the helpful comments of Aaron S. Yoshinobu and an anonymous reviewer. This study was supported by CNRS-INSU program Dynamique et Evolution de la Terre Interne (DyETI).

References

Allan, J. F., and H. J. B. Dick (1996), Cr-rich spinel as a tracer for melt migration and melt–wall rock interaction in the mantle: Hess Deep, Leg 147, *Proc. Ocean Drill. Program Sci. Results*, *147*, 157–172, doi:10.2973/odp.proc.sr.147.009.1996.

Arai, S., and K. Matsukage (1996), Petrology of gabbro-troctolite-peridotite complex from Hess Deep, equatorial Pacific: Implications for mantle-melt interaction within the oceanic lithosphere, *Proc. Ocean Drill. Program Sci. Results*, *147*, 135–155, doi:10.2973/odp.proc.sr.147.008.1996.

Ben Ismail, W., and D. Mainprice (1998), An olivine fabric database: An overview of upper mantle fabrics and seismic anisotropy, *Tectonophysics*, *296*, 145–157, doi:10.1016/S0040-1951(98)00141-3.

Blackman, D. K., et al. (2002), Geology of the Atlantis Massif (Mid-Atlantic Ridge, 30°N): Implications for the evolution of an ultramafic oceanic core complex, *Mar. Geophys. Res.*, *23*(5–6), 443–469, doi:10.1023/B:MARI.0000018232.14085.75.

Blackman, D. K., B. Ildefonse, B. E. John, Y. Ohara, D. J. Miller, C. J. MacLeod, and the Expedition 304/305 Scientists (2006), *Proceedings of the Integrated Ocean Drilling Program*, vol. 304/305, doi:10.2204/iodp.proc.304305.2006, Integrated Ocean Drill. Program, College Station, Tex.

Blackman, D. K., G. D. Karner, and R. C. Searle (2008), Three-dimensional structure of oceanic core complexes: Effects on gravity signature and ridge flank morphology, Mid-Atlantic Ridge, 30°N, *Geochem. Geophys. Geosyst.*, *9*, Q06007, doi:10.1029/2008GC001951.

Borghini, G., E. Rampone, L. Crispini, R. De Ferrari, and M. Godard (2007), Origin and emplacement of ultramafic-mafic intrusions in the Erro-Tobbio mantle peridotite (Ligurian Alps, Italy), *Lithos*, *94*, 210–229, doi:10.1016/j.lithos.2006.06.014.

Boudier, F. (1991), Olivine xenocrysts in picritic magmas—An experimental and microstructural study, *Contrib. Mineral. Petrol.*, *109*(1), 114–123, doi:10.1007/BF00687204.

Boudier, F., and A. Nicolas (1995), Nature of the Moho transition zone in the Oman Ophiolite, *J. Petrol.*, *36*, 777–796.

Boudier, F., A. Nicolas, and B. Ildefonse (1996), Magma chambers in the Oman ophiolite: Fed from the top or from the bottom?, *Earth Planet. Sci. Lett.*, *144*, 239–250, doi:10.1016/0012-821X(96)00167-7.

Bunge, H. J. (1982), *Texture Analysis in Materials Science*, 599 pp., Butterworths, London.

Burg, J. P., J. L. Bodinier, T. Gerya, R. M. Bedini, F. Boudier, J. M. Dautria, V. Prikhodko, A. Efimov, E. Pupier, and J. L. Balanec (2009), Translithospheric mantle diapirism: Geological evidence and numerical modelling of the Kondyor zoned ultramafic complex (Russian far-east), *J. Petrol.*, *50*(2), 289–321, doi:10.1093/petrology/egn083.

Cann, J. R., D. K. Blackman, D. K. Smith, E. McAllister, B. Janssen, S. Mello, E. Avgerinos, A. R. Pascoe, and J. Escartin (1997), Corrugated slip surfaces formed at ridge-transform intersections on the Mid-Atlantic Ridge, *Nature*, *385*, 329–332, doi:10.1038/385329a0.

Cannat, M. (1993), Emplacement of mantle-rocks in the seafloor at mid-ocean ridges, *J. Geophys. Res.*, *98*, 4163–4172, doi:10.1029/92JB02221.

Cannat, M. (1996), How thick is the magmatic crust at slow spreading oceanic ridges?, *J. Geophys. Res.*, *101*(B2), 2847–2857, doi:10.1029/95JB03116.

Cannat, M., D. Bideau, and R. Hebert (1990), Plastic deformation and magmatic impregnation in serpentinized ultramafic rocks from the Garrett transform fault (East Pacific Rise), *Earth Planet. Sci. Lett.*, *101*, 216–232, doi:10.1016/0012-821X(90)90155-Q.

Cannat, M., et al. (1995), Thin crust, ultramafic exposures, and rugged faulting patterns at Mid-Atlantic Ridge (22°–24°N), *Geology*, *23*, 49–52, doi:10.1130/0091-7613(1995)023<0049:TCUEAR>2.3.CO;2.

Cannat, M., F. Chatin, H. Whitechurch, and G. Ceuleneer (1997), Gabbroic rocks trapped in the upper mantle at the Mid-Atlantic Ridge, *Proc. Ocean Drill. Program Sci. Results*, *153*, 243–264, doi:10.2973/odp.proc.sr.153.013.1997.

Cannat, M., J. Cann, and J. Maclennan (2004), Some hard rock constraints on the supply of heat to mid-ocean ridges, in *Mid-Ocean Ridges: Hydrothermal Interactions Between the Lithosphere and Oceans*, *Geophys. Monogr. Ser.*, vol. 148, edited by C. R. German, J. Lin, and L. M. Parson, pp. 111–149, AGU, Washington, D. C.

Cannat, M., D. Sauter, V. Mendel, E. Ruellan, K. Okino, J. Escartin, V. Combier, and M. Baala (2006), Modes of seafloor generation at a melt-poor ultraslow-spreading ridge, *Geology*, *34*, 605–608, doi:10.1130/G22486.1.

Ceuleneer, G., and M. Rabinowicz (1992), Mantle flow and melt migration beneath oceanic ridges: Models derived from observation in ophiolites, in *Mantle Flow and Melt Generation at Mid-Ocean Ridges*, *Geophys. Monogr. Ser.*, vol. 71,

edited by J. P. Morgan, D. B. Blackman, and J. M. Sinton, pp. 123–154, AGU, Washington, D. C.

Chakraborty, S. (1997), Rates and mechanisms of Fe-Mg interdiffusion in olivine at 980°–1300°C, *J. Geophys. Res.*, *102*, 12,317–12,331, doi:10.1029/97JB00208.

Cherniak, D. J. (2007), REE diffusion in olivine, *Eos Trans. AGU*, *88*(52), Fall Meet. Suppl., Abstract MR13C-1397.

Constantin, M., R. Hékinian, D. Ackermand, and P. Stoffers (1995), Mafic and ultramafic intrusions into upper mantle peridotites from fast spreading centers of the Easter microplate (South East Pacific), in *Mantle and Lower Crust Exposed in Oceanic Ridges and in Ophiolites, Petrology and Structural Geology*, edited by R. L. M. Vissers and A. Nicolas, pp. 71–120, Kluwer Acad., Dordrecht, Netherlands.

Coogan, L. A. (2007), The lower oceanic crust, in *Treatise on Geochemistry*, vol. 3, *The Crust*, edited by K. Turekian and H. D. Holland, pp. 1–45, Elsevier, Amsterdam.

Coogan, L. A., C. J. MacLeod, H. J. B. Dick, S. J. Edwards, A. Kvassnes, J. H. Natland, P. T. Robinson, G. Thompson, and M. J. O'Hara (2001), Whole-rock geochemistry of gabbros from the Southwest Indian Ridge: Constraints on geochemical fractionations between the upper and lower oceanic crust and magma chamber processes at (very) slow-spreading ridges, *Chem. Geol.*, *178*, 1–22, doi:10.1016/S0009-2541(00)00424-1.

Dick, H. J. B. (1989), Abyssal peridotites, very slow spreading ridges and ocean ridge magmatism, in *Magmatism in the Ocean Basins*, edited by A. D. Saunders and M. J. Norry, *Geol. Soc. London Spec. Publ.*, *42*, 71–105, doi:10.1144/GSL.SP.1989.042.01.06.

Dick, H. J. B., and J. H. Natland (1996), Late-stage melt evolution and transport in the shallow mantle beneath the East Pacific Rise, *Proc. Ocean Drill. Program Sci. Results*, *147*, 103–134, doi:10.2973/odp.proc.sr.147.007.1996.

Dick, H. J. B., et al. (1999), *Proceedings of the Ocean Drilling Program, Initial Reports*, vol. 176, doi:10.2973/odp.proc.ir.176.1999, Ocean Drill. Program, College Station, Tex.

Dick, H. J. B., et al. (2000), A long in situ section of the lower ocean crust: Results of ODP Leg 176 drilling at the Southwest Indian Ridge, *Earth Planet. Sci. Lett.*, *179*, 31–51, doi:10.1016/S0012-821X(00)00102-3.

Dick, H. J. B., J. H. Natland, and B. Ildefonse (2006), Past and future impact of deep drilling in the ocean crust and mantle: An evolving order out of new complexity, *Oceanography*, *19*(4), 72–80.

Dijkstra, A. H., M. R. Drury, and R. M. Frijhoff (2002), Microstructures and lattice fabrics in the Hilti mantle section (Oman Ophiolite): Evidence for shear localization and melt weakening in the crust–mantle transition zone?, *J. Geophys. Res.*, *107*(B11), 2270, doi:10.1029/2001JB000458.

Dijkstra, A. H., M. G. Barth, M. R. Drury, P. R. D. Mason, and R. M. L. Vissers (2003), Diffuse porous melt flow and melt-rock reaction in the mantle lithosphere at a slow-spreading ridge: A structural petrology and LA-ICP-MS study of the Othris Peridotite Massif (Greece), *Geochem. Geophys. Geosyst.*, *4*(8), 8613, doi:10.1029/2001GC000278.

Donaldson, C. H. (1985), A comment on crystal shapes resulting from dissolution in magmas, *Mineral. Mag.*, *49*, 129–132, doi:10.1180/minmag.1985.049.350.19.

Drouin, M., M. Godard, B. Ildefonse, O. Bruguier, and C. Garrido (2009), Geochemical and petrographic evidence for magmatic impregnation in the oceanic lithosphere at Atlantis Massif, Mid-Atlantic Ridge (IODP Hole U1309D, 30°N), *Chem. Geol.*, *264*, 71–88, doi:10.1016/j.chemgeo.2009.02.013.

Durham, W. B., and C. Goetze (1977), Plastic flow of oriented single crystals of olivine: 1. Mechanical data, *J. Geophys. Res.*, *82*(36), 5737–5753, doi:10.1029/JB082i036p05737.

Durham, W. B., C. Goetze, and B. Blake (1977), Plastic flow of oriented single crystals of olivine: 2. Observations and interpretations of the dislocation structures, *J. Geophys. Res.*, *82*(36), 5755–5770, doi:10.1029/JB082i036p05755.

Escartín, J., and M. Cannat (1999), Ultramafic exposures and the gravity signature of the lithosphere near the Fifteen-Twenty Fracture Zone (Mid-Atlantic Ridge, 14°–16.5°N), *Earth Planet. Sci. Lett.*, *171*, 411–424, doi:10.1016/S0012-821X(99)00169-7.

Escartín, J., D. K. Smith, J. R. Cann, H. Schouten, C. L. Langmuir, and S. Escrig (2008), Central role of detachment faults in accretion of slow spreading oceanic lithosphere, *Nature*, *455*, 790–794, doi:10.1016/S0012-821X(99)00169-7.

Girardeau, J., and J. Franchetau (1993), Plagioclase-wehrlites and peridotites on the East Pacific Rise (Hess Deep) and the Mid-Atlantic Ridge (DSDP Site 334)—Evidence for magma percolation in the oceanic upper mantle, *Earth Planet. Sci. Lett.*, *115*, 137–149, doi:10.1016/0012-821X(93)90218-X.

Godard, M., et al. (2009), Geochemistry of a long in-situ section of intrusive slow-spread oceanic lithosphere: Results from IODP Site U1309(Atlantis Massif, 30°N Mid-Atlantic-Ridge), *Earth Planet. Sci. Lett.*, *279*, 110–122, doi:10.1016/j.epsl.2008.12.034.

Grimes, C. B., B. E. John, M. J. Cheadle, and J. L. Wooden (2008), Protracted construction of gabbroic crust at a slow-spreading ridge: Constraints from $^{206}Pb/^{238}U$ zircon ages from Atlantis Massif and IODP Hole U1309D (30°N, MAR), *Geochem. Geophys. Geosyst.*, *9*, Q08012, doi:10.1029/2008GC002063.

Hékinian, R., D. Bideau, J. Francheteau, J. L. Cheminée, R. Armijo, P. Lonsdale, and N. Blum (1993), Petrology of the East Pacific Rise crust and upper mantle exposed in Hess deep (eastern equatorial Pacific), *J. Geophys. Res.*, *98*, 8069–8094, doi:10.1029/92JB02072.

Holness, M. B., A. T. Anderson, V. M. Martin, J. Maclennan, E. Passmore, and K. Schwindinger (2007), Textures in partially solidified crystalline nodules: A window into the pore structure of slowly cooled mafic intrusions, *J. Petrol.*, *48*, 1243–1264, doi:10.1093/petrology/egm016.

Ildefonse, B., D. K. Blackman, B. E. John, Y. Ohara, D. J. Miller, C. J. MacLeod, and the IODP Expeditions 304–305 Scientists (2007), Oceanic core complexes and crustal accretion at slow-spreading ridges, *Geology*, *35*, 623–626, doi:10.1130/G23531A.1.

Jousselin, D., A. Nicolas, and F. Boudier (1998), Detailed mapping of a mantle diapir below a paleo-spreading center in the Oman ophiolite, *J. Geophys. Res.*, *103*, 18,153–18,170, doi:10.1029/98JB01493.

Karson, J. A., G. L. Fruh-Green, D. S. Kelley, E. A. Williams, D. R. Yoerger, and M. Jakuba (2006), Detachment shear zone of the Atlantis Massif core complex, Mid-Atlantic Ridge, 30°N, *Geochem. Geophys. Geosyst.*, *7*, Q06016, doi:10.1029/2005GC001109.

Kelemen, P. B. (1990), Reaction between ultramafic rock and fractionating basaltic magma.1. Phase-relations, the origin of calc-alkaline magma series, and the formation of discordant dunite, *J. Petrol.*, *31*, 51–98.

Kelemen, P. B., D. B. Joyce, J. D. Webster, and J. R. Holloway (1990), Reaction between ultramafic rock and fractionating basaltic magma. 2. Experimental investigation of reaction between olivine tholeiite and harzburgite at 1150°C–1050°C and 5Kb, *J. Petrol.*, *31*, 99–134.

Kelemen, P. B., et al. (2004), *Proceedings of the Ocean Drilling Program, Initial Reports*, vol. 209, doi:10.2973/odp.proc.ir.209.2004, Ocean Drill. Program, College Station, Tex.

Kelemen, P. B., E. Kikawa, D. J. Miller, and the Shipboard Scientific Party (2007), Leg 209 summary: Processes in a 20-km-thick conductive boundary layer beneath the Mid-Atlantic Ridge, 14°–16°N, *Proc. Ocean Drill. Program Sci. Results*, *209*, 1–33, doi:10.2973/odp.proc.sr.209.001.2007.

Kohlstedt, D. L., C. Goetze, W. B. Durham, and J. Vander Sande (1976), New technique for decorating dislocations in olivine, *Science*, *191*, 1045–1046, doi:10.1126/science.191.4231.1045.

Lagabrielle, Y., and M. Cannat (1990), Alpine Jurassic ophiolites resemble the modern central Atlantic basement, *Geology*, *18*, 319–322, doi:10.1130/0091-7613(1990)018<0319:AJORTM>2.3.CO;2.

Lagabrielle, Y., D. Bideau, M. Cannat, J. A. Karson, and C. Mével (1998), Ultramafic-mafic plutonic rock suites exposed along the Mid-Atlantic Ridge (10°N-30°N); symmetrical-asymmetrical distribution and implications for seafloor spreading processes, in *Faulting and Magmatism at Mid-Ocean Ridges*, *Geophys. Monogr. Ser.*, vol. 106, edited by W. R. Buck et al., pp. 153–176, AGU, Washington, D. C.

Lenoir, X., C. Garrido, J. L. Bodinier, J. M. Dautria, and F. Gervilla (2001), The recrystallization front of the Ronda peridotite: Evidence for melting and thermal erosion of lithospheric mantle beneath the Alboran basin, *J. Petrol.*, *42*, 141–158, doi:10.1093/petrology/42.1.141.

Lissenberg, C. J., and H. J. B. Dick (2008), Melt-rock reaction in the lower oceanic crust and its implications for the genesis of mid-ocean ridge basalt, *Earth Planet. Sci. Lett.*, *271*, 311–325, doi:10.1016/j.epsl.2008.04.023.

Lizarralde, D., J. B. Gaherty, J. A. Collins, G. Hirth, and S. D. Kim (2004), Spreading-rate dependence of melt extraction at mid-ocean ridges from mantle seismic refraction data, *Nature*, *432*, 744–747, doi:10.1038/nature03140.

MacLeod, C. J., R. C. Searle, B. J. Murton, J. F. Casey, C. Mallows, S. C. Unsworth, K. L. Achenbach, and M. Harris (2009), Life cycle of oceanic core complexes, *Earth Planet. Sci. Lett.*, *287*, 333–344, doi:10.1016/j.epsl.2009.08.016.

Nicolas, A., and A. Prinzhofer (1983), Cumulative or residual origin for the transition zone in ophiolites: Structural evidence, *J. Petrol.*, *24*, 188–206.

Niu, Y. (2004), Bulk-rock major and trace element compositions of abyssal peridotites: Implications for mantle melting, melt extraction and post-melting processes beneath mid-ocean ridges, *J. Petrol.*, *45*, 2423–2458, doi:10.1093/petrology/egh068.

Niu, Y., and R. Hekinian (1997), Basaltic liquids and harzburgitic residues in the Garrett Transform: A case study at fast-spreading ridges, *Earth Planet. Sci. Lett.*, *146*, 243–258, doi:10.1016/S0012-821X(96)00218-X.

Paulick, H., W. Bach, M. Godard, J. C. M. De Hoog, G. Suhr, and J. Harvey (2006), Geochemistry of abyssal peridotites (Mid-Atlantic Ridge, 15°20′N, ODP Leg 209): Implications for fluid/rock interaction in slow spreading environments, *Chem. Geol.*, *234*, 179–210, doi:10.1016/j.chemgeo.2006.04.011.

Piccardo, G. B., A. Zanetti, and O. Muntener (2007), Melt/peridotite interaction in the Southern Lanzo peridotite: Field, textural and geochemical evidence, *Lithos*, *94*, 181–209, doi:10.1016/j.lithos.2006.07.002.

Poirier, J. P., and A. Nicolas (1975), Deformation-induced recrystallization due to progressive misorientation of subgrains, with special reference to mantle peridotites, *J. Geol.*, *83*, 707–720, doi:10.1086/628163.

Rampone, E., G. B. Piccardo, R. Vannucci, and P. Bottazzi (1997), Chemistry and origin of trapped melts in ophiolitic peridotites, *Geochim. Cosmochim. Acta*, *61*, 4557–4569, doi:10.1016/S0016-7037(97)00260-3.

Rampone, E., G. B. Piccardo, and A. W. Hofmann (2008), Multi-stage melt-rock interaction in the Mt. Maggiore (Corsica, France) ophiolitic peridotites: Microstructural and geochemical evidence, *Contrib. Mineral. Petrol.*, doi:10.1007/s00410-008-0296-y.

Rosenberg, C. L., and M. R. Handy (2005), Experimental deformation of partially melted granite revisited: Implications for the continental crust, *J. Metamorph. Geol.*, *23*, 19–28, doi:10.1111/j.1525-1314.2005.00555.x.

Seyler, M., and E. Bonatti (1997), Regional-scale melt-rock interaction in lherzolitic mantle in the Romanche Fracture Zone (Atlantic Ocean), *Earth Planet. Sci. Lett.*, *146*, 273–287, doi:10.1016/S0012-821X(96)00220-8.

Sleep, N. H., and G. A. Barth (1997), The nature of oceanic lower crust and shallow mantle emplaced at low spreading rates, *Tectonophysics*, *279*(1–4), 181–191, doi:10.1016/S0040-1951(97)00121-2.

Spandler, C., H. S. C. O'Neill, and V. S. Kamenetsky (2007), Survival times of anomalous melt inclusions from element diffusion in olivine and chromite, *Nature*, *447*, 303–306, doi:10.1038/nature05759.

Sun, S. S., and W. F. McDonough (1989), Chemical and isotopic systematics of oceanic basalts: Implications for mantle composition and processes, in *Magmatism in the Ocean Basins*, edited by A. D. Saunders and M. J. Norry, *Geol. Soc. London Spec. Publ., 42*, 313–345, doi:10.1144/GSL.SP.1989.042.01.19.

Sutton, A. P., and R. W. Balluffi (1995), *Interfaces in Crystalline Materials*, *Monogr. on the Phys. and Chem. of Mater.*, vol. 51, 819 pp., Oxford Univ. Press, Oxford, U. K.

Takazawa, E., N. Abe, M. Seyler, and W. P. Meurer (2007), Hybridization of dunite and gabbroic materials in Hole 1271B from Mid-Atlantic Ridge 15°N: Implications for melt flow and reaction in the upper mantle, *Proc. Ocean Drill. Program Sci. Results*, *209*, 1–23, doi:10.2973/odp.proc.sr.209.005.2007.

Tamura, A., S. Arai, S. Ishimaru, and E. S. Andal (2008), Petrology and geochemistry of peridotites from IODP Site U1309 at Atlantis Massif, MAR30°N: Micro- and macro-scale melt penetrations into peridotites, *Contrib. Mineral. Petrol.*, *155*, 491–509, doi:10.1007/s00410-007-0254-0.

Tommasi, A., D. Mainprice, G. Canova, and Y. Chastel (2000), Viscoplastic self-consistent and equilibrium-based modeling of olivine lattice preferred orientations: Implications for the upper mantle seismic anisotropy, *J. Geophys. Res.*, *105*, 7893–7908, doi:10.1029/1999JB900411.

Tommasi, A., M. Godard, G. Coromina, J. M. Dautria, and H. Barsczus (2004), Seismic anisotropy and compositionally induced velocity anomalies in the lithosphere above mantle plumes: A petrological and microstructural study of mantle xenoliths from French Polynesia, *Earth Planet. Sci. Lett.*, *227*, 539–556, doi:10.1016/j.epsl.2004.09.019.

Tucholke, B. E., and J. Lin (1994), A geological model for the structure of ridge segments in slow spreading ocean crust, *J. Geophys. Res.*, *99*, 11,937–11,958, doi:10.1029/94JB00338.

Tucholke, B. E., M. D. Behn, W. R. Buck, and J. Lin (2008), Role of melt supply in oceanic detachment faulting and formation of megamullions, *Geology*, *36*, 455–458, doi:10.1130/G24639A.1.

Van der Molen, I., and M. S. Paterson (1979), Experimental deformation of partially melted granite, *Contrib. Mineral. Petrol.*, *70*, 299–318, doi:10.1007/BF00375359.

Vauchez, A., and C. J. Garrido (2001), Seismic properties of an asthenospherized lithospheric mantle: Constraints from lattice preferred orientations in peridotite from the Ronda massif, *Earth Planet. Sci. Lett.*, *192*, 235–249, doi:10.1016/S0012-821X(01)00448-4.

Vigneresse, J. L., P. Barbey, and M. Cuney (1996), Rheological transitions during partial melting and crystallization with application to felsic magma segregation and transfer, *J. Petrol.*, *37*, 1579–1600, doi:10.1093/petrology/37.6.1579.

Yoshinobu, A. S., and G. Hirth (2002), Microstructural and experimental constraints on the rheology of partially molten gabbro beneath oceanic spreading centers, *J. Struct. Geol.*, *24*, 1101–1107, doi:10.1016/S0191-8141(01)00094-3.